POLITECNICO DI TORINO

College of Computer Engineering, Cinema and Mechatronics

**Master's degree**
**in Cinema and Media Engineering**

Master of Science Thesis

# Helmholtz resonator Design for Optimizing Room Mode Distribution


**Tutors**
Arianna Astolfi
Marco Carlo Masoero
Monika Rychtarikova
David Jun

**Candidate**
Andrea Lai

April 2024

## Abstract

Optimizing low-frequency performance within enclosed spaces is often achieved through solutions involving acoustic absorption, including Helmholtz resonators. This thesis specifically focuses on the design of a "weakly damped" variant of these resonators, characterized by the absence of sound-absorbing material inside. The main objective is to experimentally explore and validate the differences between the effects of a real resonator and a theoretical one, also confirming a modal division phenomenon previously observed in simulations. Within the scope of this thesis, the methodology, both simulation-based and experimental, that guided the design and realization of the resonator is carefully discussed. In designing this resonator, it is crucial to identify the frequency to focus on to adjust the resonator's absorption. The work begins with the selection of a suitable environment for acoustic analysis, followed by experimental measurements and theoretical modal analysis, essential for determining the reference modal frequency. The actual design of the resonator starts with simulations that generate an accurate model of the resonator's behavior based on its fundamental properties. Thanks to the development of a custom simulation system, key parameters are estimated. This initial phase allows for outlining the design before its physical realization, culminating in an experimental phase that further refines the design. In particular, the dimensions of the holes are established through experiments with the impedance tube. After identifying the technical characteristics of the device, a piston system is implemented on the back of the resonators during the production process to allow dynamic adjustment of the cavity depth and, consequently, the resonance frequency of the resonator. Once the construction of the resonator is completed, its effectiveness is tested first in an anechoic chamber, then in the initial semi-reverberant environment, and finally in a reverberant chamber. To ensure a robust research sample, four identical resonators are produced and tested simultaneously in various configurations to assess their impact on the acoustics of the environment. Finally, the results obtained from the experimental measurements are compared with the theoretical simulations and expectations, providing a detailed analysis of the possible causes of the observed discrepancies.

# Index

# 1 Introduction

Acoustic engineering is a broad and diversified field, ranging from urban and structural acoustics to the challenges posed by room acoustics. The latter focuses on understanding and managing how sound propagates and interacts within enclosed spaces. Generally, the acoustic quality of a space depends on the direct sound from the source and the indirect reflections from surfaces. When sound encounters a surface, it can be transmitted, absorbed, or reflected, and the distribution of energy among these actions depends on the acoustic characteristics of the surface itself. Controlling this energy distribution, and particularly the reflections, is a key aspect in acoustics.

Effective architectural acoustic design requires appropriately sized rooms, suitable shapes, and surface treatments through a balanced mix of absorbers, diffusers, and flat surfaces for managing reflections. Absorbers and diffusers are both crucial to prevent acoustic distortions such as echoes, colorations, and shifts in the sound image due to strong reflections. The optimal choice between absorbers and diffusers, and the appropriate type of absorbing or diffusing device, depends on several factors, including the need to reduce reverberation time and/or sound level, as well as the nature of the environment.

In spaces like concert halls, where acoustic energy is essential, diffusers are often preferred. In smaller environments, such as lecture halls where intelligibility is a priority, a balance is sought between absorption to regulate reverberation time and sound level, and diffusion to ensure that early reflections are helpful without causing distortions. In critical listening rooms, a combination of absorbers and diffusers is employed to optimize the acoustics of the space.

Every room, with its size, shape, geometry, and construction materials, exhibits standing wave resonance, known as modes. These are the specific resonance frequencies of the environment, and their effective management is crucial to ensure sound comfort. Managing low frequencies is particularly complex due to their long wavelengths relative to room dimensions and the greater associated energy, which can cause excessive reverberation and unwanted sound colorations. The control of these low-frequency modes typically occurs through absorption; however, porous absorbers like polyurethane foam, cellular melamine, fiberglass, and fluffy fabrics [1, 2, 3, 4, 5] can prove inadequate due to poor absorption at low-frequency regime. Therefore, resonant absorbers, more compact and positionable at strategic points, are often preferred.

However, unlike porous materials, achieving broadband absorption in a single device is challenging, so one of the common challenges in designing resonant structures is to extend the bandwidth. There are three common forms of the device: the first is the Helmholtz absorber [6, 7, 8, 9, 10], named after the German physicist and physician Hermann von Helmholtz (1821–94), the second is the micro-perforated panel [11, 12, 13, 14, 15, 16, 17, 18, 19] and the third is a membrane or panel absorber [20]. The ideas and concepts of resonant absorption have been known for many decades. In recent years, some more specialized devices, such as transparent absorbers, have been produced, but these still rely on the same basic physics. While for some devices, such as various standard Helmholtz absorbers, there is the possibility of calculating their effectiveness with reasonable precision, for others, for example, those based on membranes, the design still largely relies on experimental methodologies. These treatments are commonly employed to address the low-frequency modes of the room and as parts of silencers within ventilation systems.

Among the various types of absorbers, Helmholtz resonators (HRs) represent an effective solution for addressing low-frequency problems. Traditionally, these resonators are equipped with porous absorbing material inside to achieve the losses necessary for removing sound energy. Besides them, there also exists an undamped variant, which does not utilize porous materials, and which comes with less common reflection characteristics.

This thesis project focuses on this specific variant of the HR, exploring its potential and limitations in the field of indoor acoustics. Through a combination of theoretical analysis and

experimental testing, the goal is to understand how this particular configuration of the resonator affects the absorption of low frequencies and what are the practical implications of its use in real environments. The design of these resonators involves finding the optimal combination of four key parameters: cavity depth, thickness of the perforated panel, hole sizes, and hole distribution. This thesis describes in detail the procedure for estimating these parameters and the methodologies employed to evaluate their effectiveness.

The research aims to experimentally validate the behavioral differences between theoretical and real resonators, with a specific focus on a modal splitting phenomenon previously observed in simulations [21]. This thesis makes a significant contribution to the field of acoustic engineering, proposing new perspectives on the treatment of low frequencies in enclosed spaces and highlighting the importance of HRs in acoustic design.

In the following sections, the thesis will examine in detail the theoretical context, review the existing literature, and explain the methodology adopted for the research, including the design, production, and testing of 'weakly damped' resonators. The results will be critically analyzed, offering an in-depth view of this approach to acoustic optimization.

## *1.1 Therminology*

This section introduces key concepts and quantities in acoustics, essential for analyzing sound propagation and interaction.

### 1.1.1 Frequency $f$ [Hz]

Frequency, as an acoustic quantity, refers to the number of oscillations a sound wave completes in one second.

### 1.1.2 Frequency Spectrum

The frequency spectrum illustrates the distribution of energy or intensity of an acoustic signal across its frequency components, highlighting how a property of the wave varies with frequency. This representation, obtainable through Fourier transform, provides a detailed view of the frequency components that make up the signal.

### 1.1.3 Sound

Sound can be defined as the audible part of the frequency spectrum of acoustic signal. The limits of this range are highly subjective and change with age, but the most commonly cited range is 20–20000 Hz.

### 1.1.4 Speed of sound $c$ [m.s$^{-1}$]

The speed of sound in air, considered as an ideal gas, is determined by a thermodynamic relationship. In solids, sound propagates very quickly, while in gases, the speed is slower. For common room temperature values, an approximation of the relationship given by

$$c = 331.4 + 0.6t \tag{1}$$

can be used, with $t$ representing the temperature in degrees Celsius.

### 1.1.5 Angular frequency $\omega$ [s$^{-1}$]

In the context of waves, such as sound or electromagnetic waves, the angular frequency represents how many times the wave completes a full cycle (i.e., $2\pi$ radians) in one second. The relationship between angular frequency $\omega$ and frequency $f$ is given by the formula:

$$\omega = 2\pi f \tag{2}$$

### 1.1.6 Wavelength $\lambda$ [m]

The wavelength is the distance a sinusoidal wave travels in one period $(1/f)$ and is usually measured in meters (m). In acoustics, the wavelength is often used to describe the frequency of

sound, where longer wavelengths correspond to lower frequencies and shorter wavelengths correspond to higher frequencies. The corresponding equation is:

$$\lambda = \frac{c}{f} \tag{3}$$

1.1.7 Wave number $k$ [$m^{-1}$]

The wave number is the reciprocal of the wavelength and expresses the number of wavelengths per unit length. It can assume both real and complex values and is represented by the fundamental relation:

$$k = \frac{\omega}{c} \tag{4}$$

The relationship between wavelength ($\lambda$) and wave number ($k$) can alternatively be expressed as:

$$k = \frac{2\pi}{\lambda} \tag{5}$$

1.1.8 Characteristic acoustic impedance $Z_c$ [Pa.s.$m^{-1}$, Rayls]

A quantity with a meaning analogous to impedance in an electrical circuit [22], very useful property of the material when calculating the transmission of acoustic waves within and between different acoustic media. The characteristic impedance ($Z_c$) along with the wave number ($k$) characterizes the propagation of sound through the material, and it has a close connection with the pressure and particle velocity described by:

$$p = Ae^{j(\omega t - kx)} \tag{6}$$

$$u = \frac{A}{\rho c} e^{j(\omega t - kx)} \tag{7}$$

The characteristic specific acoustic impedance of the medium, $Z_c$ and corresponds to the ratio between pressure ($p$) and particle velocity ($u$). It can be expressed by the formula:

$$Z_c = \rho c \tag{8}$$

At room temperature and standard atmospheric pressure, the acoustic impedance of air is about 415 rayls.

1.1.9 Surface acoustic impedance $Z$ [Pa.s.$m^{-1}$, Rayls]

The surface impedance reflects the response of a material surface to the incidence of sound, considering how sound waves are reflected, absorbed, or transmitted by that surface. It is often split into the real term (resistance) and imaginary term (reactance). A simple inspection of the surface acoustic impedance gives more insight into the absorbing properties of a material than the absorption coefficient.

In the case of a resonant system, the surface impedance can be expressed through the following relationship [22]:

$$z = r_m + j[\omega m - \rho c \cot(kt)] \tag{9}$$

where $k$ is the wave number in the air; d is the depth of the cavity; m is the acoustic mass per unit area of the panel, and rm represents the resistance term associated with energy losses.

1.1.10 Kinematic viscosity of air $v$ [$m^2s^{-1}$]

Kinematic viscosity of air refers to a measure of the air's resistance to flow and shear within itself or past solid objects. It is a specific type of viscosity that considers the fluid's (in this case, air's) density. At standard atmospheric pressure and temperature, the kinematic viscosity of air is approximately $15 \times 10^{-6}$ $m^2s^{-1}$.

1.1.11 Density of air $\rho$ [$kg.m^{-3}$]

At standard atmospheric pressure and temperature, the density of air is approximately 1.225 $kg/m^3$.

1.1.12 Acoustic Pressure $p_t$ [Pa]

The instantaneous acoustic pressure *pt* is a quantity dependent on time and space that expresses the difference between the total pressure ($p$) and the barometric pressure ($p_s$).

$$p_t = p - p_s \tag{10}$$

1.1.13 Reflection Coefficient $R$ [−]

It is the ratio between the reflected acoustic pressure and the incident acoustic pressure in relation to the considered structure [22]:

$$R = \frac{p_r}{p_i} \tag{11}$$

1.1.14 Acoustic Absorption Coefficient $\alpha$ [−]

This quantity generally expresses the ratio between the absorbed energy and the incident energy. It can be calculated from the reflection coefficient $R$ using the relationship [22]:

$$\alpha = 1 - |R|^2 \tag{12}$$

1.1.15 dBFS

dBFS is a unit of measurement that indicates the level of an audio signal relative to the maximum possible level without distortion in a digital system. The maximum possible level, known as "full scale," corresponds to 0 dBFS, which represents the maximum amplitude that a digital signal can have without incurring clipping. The calculation of a signal's level in dBFS is expressed by the formula:

$$L_{dBFS} = 20\log\left(\frac{A_{signal}}{A_{max}}\right) \tag{13}$$

where $A_{signal}$ is the amplitude of the signal in question and $A_{max}$ is the maximum possible amplitude without distortion.

1.1.16 Reverberation Time $T$ [s]

Defined as the time during which the level of acoustic pressure decreases by 60 dB after the sound source is turned off, with variants like *T20*, *T30*, and *EDT* depending on the part of the reverberation curve considered. It can be calculated using Sabine's formula [23]:

$$T_{60} = \frac{55.3V}{cA}, \tag{14}$$

where $V$ is the room volume and $A$ the total absorption of all room surfaces.

The total absorption of the room can be calculated from the individual absorption coefficients of the room surfaces, using the following expression:

$$A = \sum_{i=1}^{N} S_i \alpha_i = S\bar{\alpha} \tag{15}$$

where $S$ is the total surface area of the room and $\bar{\alpha}$ is the weighted average absorption coefficient of the room with respect to surface areas.

Sabine's formulation does not correctly predict the reverberation time for rooms with a large amount of absorption. So, over the years, many new formulations have been developed. Among these, the most popular is the Eyring-Norris equation [24]. Meanwhile, the Millington equation [25] gains significance in the context of reverberation chamber experiments.

## *1.2 Room acoustics*

Room acoustics is a branch of physics and engineering that deals with the study and control of sound in indoor spaces. This field has roots that go back centuries, but it was in the 20th century that it saw significant developments thanks to technological advancement and a growing awareness of the importance of sound and its impact on living spaces.

Since ancient times, acoustics was already a key element for architects and builders, as demonstrated by Greek and Roman theaters, designed with a marked awareness of sound dynamics. This sensitivity extended into the Middle Ages, with Gothic cathedrals optimized to enhance the sonority and clarity of choirs. Later, the Renaissance and the Enlightenment fueled a renewed interest in science and mathematics, leading figures like Leonardo da Vinci and Galileo Galilei to expand the field of acoustics. However, it was only in the 19th century that acoustics was established as an independent scientific discipline, thanks to the contributions of scientists such as Hermann von Helmholtz and Lord Rayleigh. The following century witnessed significant advances in the field, driven by the need to improve acoustics in public places and performance arenas. Innovations, both theoretical and technological, led by pioneers such as Wallace Clement Sabine, the father of modern architectural acoustics, introduced scientific methods for acoustic design and evaluation.

The main objectives of room acoustics are numerous and include improving speech inteligibility in spaces such as classrooms and conference rooms, optimizing acoustic conditions for musical performances in theaters and concert halls, and creating comfortable environments by reducing unwanted noise levels. Considering the negative impact that noise can have on the physical and psychological state of the individual, as highlighted by the most recent studies, ensuring a comfortable and health-promoting environment becomes even more important [26, 27, 28, 29, 30, 31, 32, 33, 34]. The issue is particularly pronounced in the low-frequency range, as sound energy can cover greater distances and sound insulation is less efficient [35]. Besides, noise has a detrimental impact on the stability and operation of instruments, machines, and other structures [36]. These challenges are addressed through careful balancing of sound absorption, reflection, and diffusion within spaces, to create sonic environments that meet specific functional and aesthetic needs. Achieving these objectives involves overcoming various challenges that depend on the nature of the space and its intended functions. These include managing external noise, controlling reverberation and unwanted echoes, and acoustic isolation between adjacent spaces. The complexity of the interactions between sound waves and internal surfaces requires a deep understanding of physical principles and careful design to achieve optimal results.

In the acoustic design of environments, it is essential to consider not only the physical properties of the space but also the activities that will take place there and the expectations of the users. This holistic approach ensures that acoustic solutions not only solve technical problems but also enhance the overall experience of the occupants, raising the quality of their time spent in such environments.

### 1.2.1 Sound propagation

Room acoustics is based on physical principles that govern the dynamics of sound, which propagates through various mediums (such as air, liquids, and solids) in the form of longitudinal waves. These sound waves exhibit characteristics such as frequency, wavelength, speed, and intensity, which play a fundamental role in human auditory perception.

When sound waves encounter surfaces or obstacles, they can be transmitted, absorbed, or reflected, and the way this occurs depends on the acoustic properties of the encountered object. In the case of transmission, the sound passes through the object, carrying sound energy into a new environment, which has direct implications for the acoustic insulation between two distinct spaces. Absorption occurs when a surface captures sound energy, converting it into heat, leading to a decrease in the intensity of the reflected sound. Regarding reflection, it occurs when sound waves are bounced back by the surface. This phenomenon can manifest as specular reflection, when the sound is uniformly reflected by wide and smooth surfaces, or as diffuse reflection, which occurs when the sound is distributed more evenly in space and time by surfaces acting as acoustic diffusers, contributing to a more homogeneous sound distribution in the environment. **Figure 1** illustrates temporal and spatial characteristics of absorbing, specularly reflecting and diffusing surfaces, which form the acoustical palette. In addition to the surface types shown in the **Figure 1**, there are also hybrid surfaces, which can both absorb and diffuse to varying degrees.

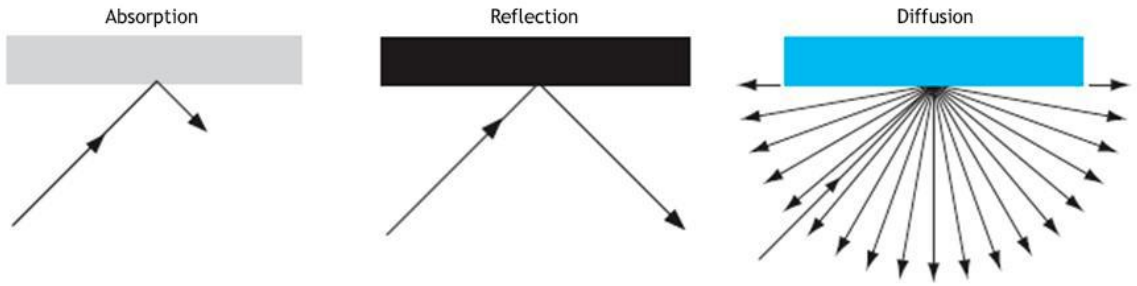


**Figure 1**: Acoustic effects of absorptive, reflective, and diffusive surfaces

Within a room, the sound perceived at a given point is the result of the interaction between the direct sound emitted by a source and the resulting reflections (see **Figure 2**). These reflections are influenced by the structure and geometry of the room, elements that have a significant impact on the internal sound field.

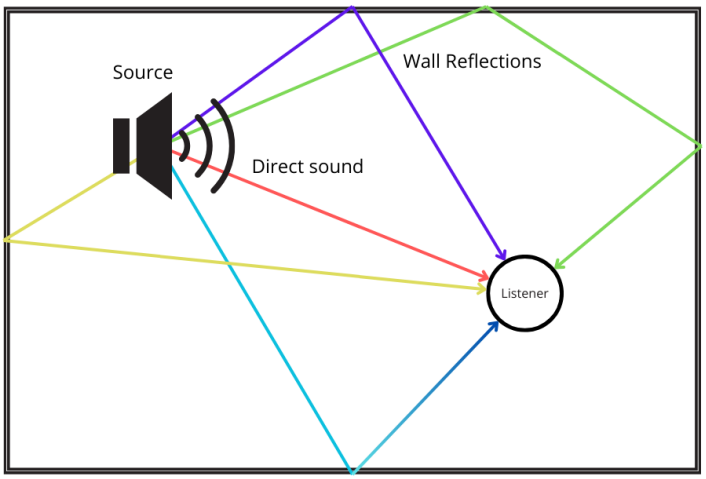


**Figure 2**: A typical example of sound reflections within a rectangular room

However, the sound field within a closed space is so complex that it eludes precise mathematical analysis, due to the high number of variables involved, such as modes and sound reflections. This complexity makes the exact calculation of the sound field a challenging

endeavor, and the results of such calculations, even if possible, would be too intricate to be practically useful. Consequently, approximations and simplifications that condense the data into averages or manageable functions are necessary, often relying on statistical methods and models.

However, these simplifications must align with the properties of human hearing, implying that advancements in environmental acoustics are closely dependent on progress in psychoacoustics. The relationship between objective acoustic stimuli and subjective perceptions, therefore, continues to require empirical investigation, awaiting a deeper understanding of the physiological and psychological mechanisms of hearing. Moreover, the very nature of acoustic perception, influenced by highly subjective factors such as personal tastes and individual predispositions, highlights the impossibility of defining a unique "ideal acoustic environment".

This variability in perception is reflected in the diverging opinions regarding the acoustics of concert halls, highlighting how different spaces can be considered excellent by different audiences. This diversity, far from being a limitation, enriches the field of environmental acoustics, presenting both challenges and opportunities for study and appreciation.

In the context of this thesis, reporting the mathematical considerations that would describe the dynamics of the sound field is not of primary interest. What is important is to recognize that the acoustic response of a room becomes more predictable if the room has a uniform geometry.

### 1.2.2 Room modes

When a rectangular room is acoustically excited by a sinusoidal signal that matches the room boundary conditions in a specific way, standing wave resonance appears, commonly referred to as room mode [37]. As previously anticipated, this phenomenon depends on the shape, size, and construction materials of the environment. These modes occur due to the reflections of sound waves from the walls, ceiling, and floor, manifesting as accumulations of sound energy at certain frequencies, causing an uneven distribution of sound in the room. As a result, some frequencies may be perceived as emphasized in certain areas, while in others they may be attenuated or almost imperceptible. Moreover, depending on the walls involved in the reflections, the energy distribution assumes a different configuration, and the mode is classified as axial, tangential, or oblique (see **Figure 3**).

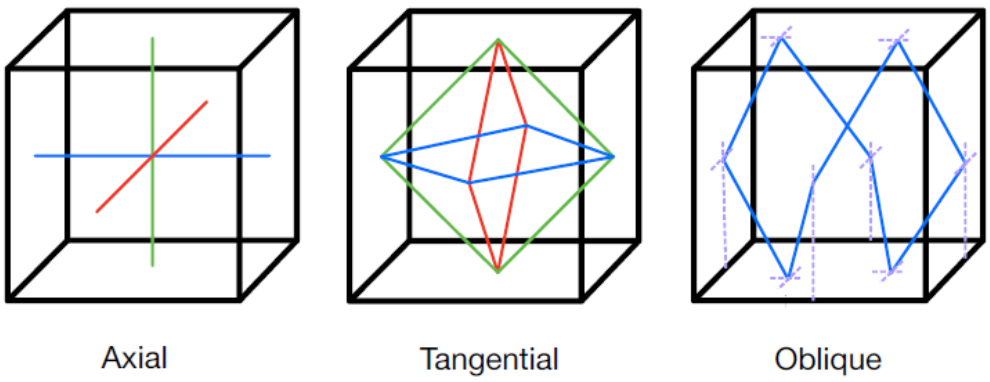


**Figure 3**: Representation of the modes of a room

Rooms with simple geometric shapes make mathematical simulations easier. The modes within rectangular enclosed rooms can be described with an x-y-z triplet. This triplet represents a three-dimensional Cartesian coordinate system. Each axis of the triplet (x, y, z) corresponds to one of the three main spatial dimensions of a room: width (x), depth (y), and height (z). These axes are perpendicular to each other and define a reference point from which to measure positions and distances within the considered space.

In the description of the modes of a room, such as in the case of an axial mode 1-0-0, these numbers are indicators of specific resonance modes within the room, based on the number of half-wavelengths (or nodes) present along the room's dimensions (width, height, and depth, corresponding to the x, y, and z axes).

Axial modes occur along a single dimension (such as 1-0-0, 0-1-0, or 0-0-1). These are the simplest and produce the lowest resonance frequencies. Tangential modes involve two dimensions (such as 1-1-0, 0-1-1, etc.), and have resonance frequencies slightly higher than axial modes. Oblique modes involve all three dimensions (such as 1-1-1) and produce the highest resonance frequencies. The frequency at which a mode resonates is called its eigenfrequency [38, 39].

As will be shown later, the calculation of the resonance frequencies of a rectangular room can be done based on its dimensions. Although perfectly rectangular rooms are rare, many concert halls, churches, and classrooms closely resemble a rectangular shape more than any other simple geometry. As a result, findings obtained for strictly rectangular environments can be applied, at least qualitatively, to many of the rooms encountered in practice.

Although the analysis of the room's natural vibration modes provides a fundamental understanding of its acoustic response at low frequencies, it's important to recognize that the acoustic behavior of a space is not limited exclusively to these modal phenomena.

Once a certain frequency threshold, known as the Schroeder frequency, is surpassed, there's a significant shift in sound distribution within the space.

The Schroeder frequency marks the transition from modal to diffuse regime, wherein sound waves begin to interact with the room's surfaces in a more complex manner, resulting in multiple reflections and overlays that generate a diffuse sound field. In this regime, sound is distributed more evenly throughout the space, making the listening experience less dependent on the listener's or sound source's specific location compared to the low frequencies dominated by modal resonances. To calculate the Schroeder frequency [40, 41] of a room, the following formula can be used:

$$f_s = 2000\sqrt{\frac{T_{60}}{V}} \tag{16}$$

where $f_s$ represents the Schroeder frequency in Hertz (Hz), $T_{60}$ is the reverberation time (in seconds), $V$ is the volume of the room in cubic meters (m³), and $c$ is the speed of sound in air (approximately 343 m/s at room temperature).

In large halls, the Schroeder frequency typically lies between 20 and 30 Hz, leading to significant modal overlap across the entire frequency spectrum of interest. This makes the analysis of individual natural frequencies superfluous. Conversely, in smaller rooms, a portion of the relevant frequency range falls below the Schroeder frequency. For example, in a classroom of 200 m³ with a reverberation time of 1 second, the Schroeder frequency is about 140 Hz, with approximately 60-70 natural modes dominating the acoustic behavior below this threshold. This observation highlights the paradox that the acoustics of small rooms can be more complex than those of large halls.

Confined spaces often encounter issues with low-frequency modes, where stationary modes manifest as distinct peaks along the frequency axis. This non-uniform distribution causes some frequencies to be reinforced where the modes are strong, while others are diminished where the modes are weak. This is especially critical for musical applications, particularly with the increasing use of subwoofer technology and the playback of modern music with a high bass content.

To address these acoustic issues, commonly adopted strategies include carefully selecting the room's dimensions and the placement of speakers and listening positions, aiming to even out the frequency response and prevent problematic acoustic modes. Despite this, additional acoustic treatments are often necessary, as the frequency response tends to remain uneven. Pronounced low

modes require specific interventions, such as the use of bass traps, since traditional porous absorbers are not effective for low frequencies unless they are particularly thick. Consequently, resonant absorbers are preferred for treating low frequencies, thanks to their ability to interact with the associated wavelengths more effectively.

## *1.3 Helmholtz resonator*

Resonant absorbers are mass-spring systems with damping designed to achieve absorption at low (<500 Hz) and medium frequencies (500-2000 Hz). The absorption characteristics of these resonant devices feature an absorption peak. Unlike porous materials, achieving broadband absorption with a single resonant device is challenging, hence expanding the bandwidth is a common problem in the design of resonant structures. As we will discuss further, modern researchers are actively exploring innovative approaches to overcome this challenge, seeking to enhance the performance and versatility of resonant absorbers in a variety of applications.

As previously mentioned, there are primarily three types of resonant device: the Helmholtz resonator (HR) and the membrane absorber, illustrated in **Figure 4**. Resonant absorbers involve a mass vibrating against a spring. In the case of a Helmholtz absorber, the mass consists of an air column inside the opening of a perforated sheet. The principle of resonance is the same that occurs when blowing over the opening of a beer bottle, generating a musical note. To convert it into an absorbing device, the energy losses necessary to eliminate sound energy are introduced through damping, which is commonly achieved with the use of a layer of mineral wool. At the resonance frequency, speed of air molecules in the neck is maximum, and associated viscous and thermal losses due to forces acting on these air molecules are also maximum, which results in the maximum damping of incident acoustic waves [42]. While the mass of the MPPs also corresponds to the air columns inside the panel holes, for a membrane absorber, the mass is a vibrating sheet of material such as rubber, mass-filled vinyl, or plywood. In each case, the spring is provided by the air enclosed in the cavity. By changing the vibrating mass and the stiffness of the air spring, it is possible to tune the resonance frequency of the device, and it is at the resonance frequency that absorption is maximized.

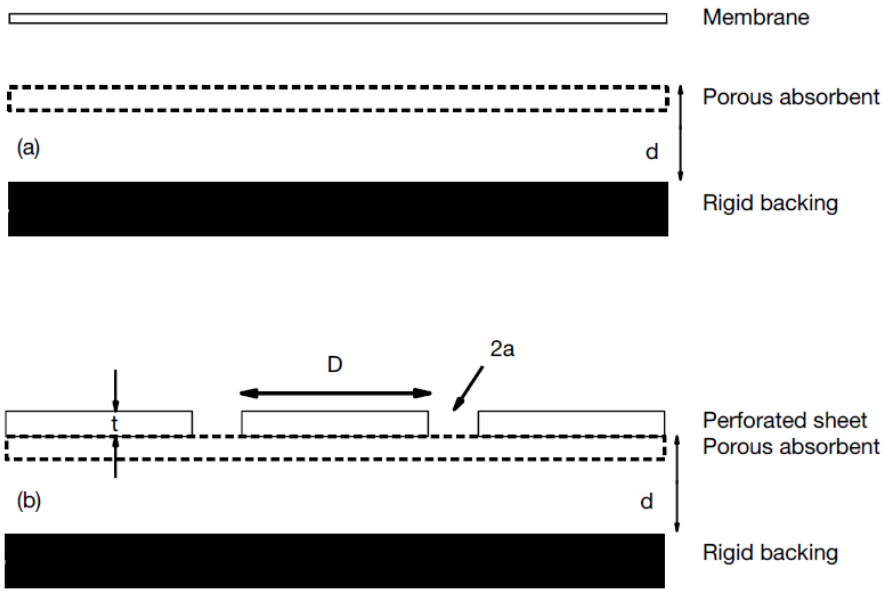


**Figure 4**: Typical constructions for (a) membrane, and (b) Helmholtz absorbers

To achieve damping, porous absorbing material is often placed where the particle velocity is high, that is, in the neck of the HR or right behind the membrane in the panel absorber. In the latter case, the absorbent should not be so close as to inhibit the movement of the membrane.

Alternatively, for Helmholtz devices with small openings, viscous losses within the neck can be used to achieve absorption; this is a technique that allows to produce devices without porous absorbent, such as microperforated absorbers.

Unlike a membrane absorber, whose design primarily requires an experimental and empirical approach, the behavior of a HR can be anticipated thanks to design equations. The main parameters of these equations are illustrated in Figure 1.4b and correspond to *t* (thickness of the perforated panel), *d* (depth of the cavity), *D* (repetition distance between the holes), and *a* (radius of the holes).

The dimensions of the resonator and the holes on the front panel significantly influence the device's performance. As the sizes of the holes increase, the open area expands, which leads to an increase in the resonance frequency. Additionally, increasing the cavity depth *d* reduces the stiffness of the "air spring," causing a decrease in the peak absorption frequency. Regarding the cover panel, its perforated surface is divided into individual cells that are assumed to act independently of each other. The hole configuration, arranged on two perpendicular axes, ensures uniformity with a constant repetition distance *D* in every direction, as represented in **Figure 4**. Furthermore, to optimize the resonator's effectiveness, it is essential that the distance between the holes is significantly greater than their diameter. Finally, the panel's thickness *t* and the hole's radius *a* are considered much smaller than the wavelength of sound in the air.

Nonetheless, choosing a suitable material for constructing the device is necessary. Currently, wood is often the preferred surface treatment in general architectural spaces, as well as in critical listening and performance spaces. Alternatively, Helmholtz absorbers are constructed with cores of medium-density fiberboard (MDF) (see **Figure 5**), which is cheaper and easier to work with than wood. The resonator should be reasonably rigid; therefore, it's important that the boards have an adequate thickness.

**Figure 5**: Industrial MDF panels

### 1.3.1 Recent advancements

The Helmholtz Resonator has traditionally been used in mitigating low-frequency, monotonous noise. However, there has recently been innovative effort aimed at extending its absorption bandwidth despite numerous challenges encountered. A standard configuration of a HR is characterized by its small size relative to the working wavelength, typically set to $\lambda/4$, demonstrating a marked absorption peak in a narrow band at low frequencies. However, since the absorption effectiveness is influenced by the depth of the cavity, it often still needs to be considerable.

Following initial theoretical analyses on traditional HRs, several studies have focused on the development of innovative HR structures through modifications to the shape and size of the neck

and cavity. One strategy to reduce the thickness of the absorber without compromising its efficiency has included altering the neck geometry, with solutions such as the extended neck [43], inserted neck [44], spiral neck [45], and conical neck [46].

Alster [47] formulated the resonance frequencies for HR structures of various shapes, such as sphere, prism, cone, toroid, etc., considering the air mass present in the neck and cavity. Concurrently, some studies investigated the acoustic behavior of HRs with unconventional geometries. The resonance frequency of an HR with a rectangular parallelepiped cavity was examined, and a mathematical model was proposed by Chanaud [48].

Selamet and colleagues [49] explored the resonance frequency and attenuation properties of concentric HRs, opening new research avenues in the field. Subsequently, they delved into the study on the attenuation behavior and resonance frequency of asymmetric HRs [50], introducing a three-dimensional analytical method to analyze the propagation of non-planar waves at the interface between neck and cavity. Randeberg [51] proposed a new HR configuration with the neck extended laterally, which, compared to traditional HRs, showed a notable increase in viscous losses. Komkin [9], for his part, conducted an in-depth investigation to characterize the acoustic absorption properties of HRs, establishing through analytical and experimental research a relationship between geometric factors and the absorption properties of HRs. The experiment was carried out by placing an HR on the end wall of a circular duct and varying the diameter and length of the resonator's neck, as well as the depth of the cavity. Although it was not conceived in the context of room acoustics study, this research can draw very important general conclusions. Komkin demonstrated that the viscous loss at the neck edges increases as the neck diameter decreases, weakly depends on the neck length until it exceeds the diameter of the neck, and significantly decreases with the increase of the depth of the cylindrical resonator's cavity when the cavity depth becomes much smaller than the diameter of the resonator's cavity.

This growing interest in absorbing a wider range of frequencies has led to a revisitation of the classical HR concept, favoring the adoption of composite structures integrating various HR configurations. To meet this challenge, the scientific community has examined a wide variety of combinations, including HR arrays [7], demonstrating significant potential in overcoming traditional limits through innovation and experimentation with new geometries and configurations.

Research has confirmed that resonant absorbers based on HR arrays with variable resonance frequencies are capable of effectively absorbing sound across a wide range of frequency spectra [44, 52, 53, 54]. These HR arrays can be optimized to act as acoustic barriers, offering optimal performance in noise transmission. Some HR designs do not achieve complete sound absorption at their resonance frequencies, thus termed "imperfect" resonators. Although the absorption peaks of "imperfect" HRs are lower than those of "perfect" resonators, their absorption curves are more extended, allowing them to cover a wider frequency range. This characteristic makes them particularly effective in combination with adjacent HRs that have similar resonant frequencies, allowing for a greater overlap of frequencies [53, 55]. It is crucial, however, that these systems are designed carefully to ensure that their mutual interaction enhances, rather than hinders, the overall performance.

Further configurations explored include multi-layer HRs [56], HRs coupled with micro-perforated panels (MPP) [57], HRs integrated with porous materials [58, 59], and acoustic metamaterials incorporating HRs [60]. Among these, acoustic metamaterials based on HRs represent a promising frontier for future research in the field of acoustics. The relatively new concept called acoustic metamaterials or metasurfaces has been applied to achieve extraordinary absorption at low frequencies with absorber sizes smaller than the wavelength [61, 62, 63, 64, 65, 66, 67, 68, 69, 70].

These advanced structures offer broad-band absorption at low frequencies with reduced thickness, marking a significant advancement in acoustic engineering. HRs and designs based on these technologies find application in a variety of fields, including environmental acoustics [37],

the automotive sector [71, 72], cargo fairings [73], and the aerospace industry [74, 75], highlighting their versatility and potential impact across different sectors.

Thanks also to the simplicity of fabrication, research on acoustic metasurfaces aimed at achieving "perfect" sound absorption (over 99% absorption of sound energy) through hybrid resonance between coupled HRs has gained momentum [62]. For instance, in 2016, an acoustic metasurface capable of perfect sound absorption at a specific frequency was introduced, exploiting the hybrid resonance between two adjacent HRs [63], and in recent years studies on this subject have been periodically updated.

In particular, very recent research presented at the Forum Acusticum 2023 [76] proposed a thin acoustic metasurface for broad-band sound absorption based on hybrid resonances at multiple target frequencies. The supercells of the proposed metasurface were subdivided into multiple unit cells, each consisting of two sub-wavelength adjacent HRs to induce hybrid resonance due to wave trapping phenomena near the metasurface and destructive interference between reflected waves in the far field.

The advancement in research on acoustic metasurfaces, characterized by significant progress and innovations, further underlines the central role of the HR in the field of acoustic engineering. This evolution demonstrates how the fundamental principles of the HR continue to influence and inspire the new frontiers of acoustic technology, confirming its indispensable role in research and development of innovative solutions for sound manipulation.

## *1.4 Anechoic Chamber*

Certain types of acoustic measurements, such as microphone calibration, determination of sound source directional patterns, or psychoacoustic experiments, require highly accurate and reliable results that cannot be compromised by the interference of direct sound with sound components reflected from boundaries. To avoid sound reflections — except those from the ground — one solution could be to conduct measurements or experiments in open environments. This approach, however, carries the risk of heavily depending on favorable weather conditions, necessitating not just the absence of rain but also wind, and also poses the risk that external environmental noise could interfere with the acoustic measurements.

An effective solution to these challenges is the use of a so-called anechoic chamber, an acoustically dead space, an extreme example of acoustic absorption. This environment is designed with surfaces that, above a certain cutoff frequency, ensure almost total sound absorption with an absorption coefficient exceeding 0.99 at every angle of incidence. This requirement cannot be met with uniform flat layers of absorptive material; instead, a wall coating is needed that creates a gradual or continuous transition of the characteristic impedance from that of air to that of a highly dissipative material. This transition is commonly achieved using porous wall coatings, which progressively increase their resistance to air flow. It's important to note that, in the presence of sounds arriving tangentially to the surface, a uniform plane might not absorb the sound due to total reflection. Therefore, adopting solutions based on complex geometries, such as the installation of pyramids or wedges made of open-cell foam or fiberglass, is preferable. These structures, by introducing absorption channels that progressively narrow, ensure that incident sound waves are effectively absorbed without generating significant reflections. The effectiveness of these absorption systems is guaranteed when the length of the channels, or the thickness of the coating, is at least a third of the acoustic wavelength, a condition more easily met at higher frequencies. As a result, every anechoic chamber has a lower cutoff frequency, below which the absorption coefficient of the walls is less than 0.99.

The floor, like the walls, requires such treatment, supported by an elevated structure that allows access to the room without affecting its acoustic properties. Integrating cavity resonators between the wedges and the rigid wall further reduces the lower frequency limit, expanding the range of frequencies manageable by the environment [14]. **Figure 6** shows the anechoic chamber at KU Leuven.

**Figure 6**: The anechoic chamber at KU Leuven

## *1.5 Reverberation room*

While the anechoic chamber provides a critical environment completely free of echoes, on the other hand, the reverberation chamber is positioned, where reflections are maximized to ensure a uniformly diffused sound field within the space.

Reverberation plays a crucial role in room acoustics, often being considered the least disputable standard for assessing the acoustic properties of enclosed spaces. There is a profound connection between reverberation and sound diffusion: the dynamics of reverberation are only explained in scenarios where sound propagates in all directions with uniform intensity, both in stationary situations and during the sound's decay, at least on average over short intervals compared to the total decay time. Obviously, in practice, these ideal conditions are only approximately achievable. Despite this, excellent sound diffusion can be achieved in certain rooms designed for measurements, such as reverberation chambers, which provide an ideal environment for testing specific devices like resonators.

To achieve this condition, reverberation chambers are usually equipped with diffusers scattered throughout the space, and their walls are designed with specific inclinations to avoid parallelism (see **Figure 7**).

**Figure 7**: The reverberation room at KU Leuven

Additionally, these rooms must have certain dimensions and a low inherent absorption. However, since the reverberation time can vary based on the position inside the room, it is

common practice to place sound sources and microphones in multiple points and calculate an average of the results to minimize discrepancies due to non-ideal diffusion. Typically, the sound source is positioned in a corner of the room, aimed at the corner itself, to enhance the activation of room modes while minimizing the direct sound from the speaker reaching the test material [22]. The microphones need to be positioned at least 1 meter away from any walls, the room's diffusers, and the material being tested, to achieve a varied sampling of the room's volume. Even with all these measures, the measured absorption coefficients are often less accurate at low frequencies than at high frequencies due to modal effects. Moreover, the evaluation must be carried out on samples of considerable sizes, which is a necessity for certain construction scopes but may result in unjustified expenditure for others. It is also important to underline that the consistency of the measured results generally presents a low level of repeatability. An additional significant limitation concerns the inability to determine the acoustic impedance, leading researchers in the field of absorbent materials to prefer the use of the impedance tube to study the properties on small samples before proceeding with broader tests in reverberation chambers.

## *1.6 Impedance Tube*

The impedance tube, or standing wave tube, plays a key role in validating predictive models, offering the possibility to measure both the normal incidence absorption coefficient and the surface impedance of materials [77, 78].

The impedance tube (see **Figure 8**) consists of a tube, inside which the sample to be tested is placed, and a sound generator located at the opposite end. This configuration can vary in terms of the tube's shape, which can be rectangular or circular, and includes a loudspeaker that emits sound waves directed towards the sample. To reduce resonances, it may be advantageous to place an absorbent material in front of the loudspeaker, although this is not strictly necessary [22]. The sound reflection from the sample generates partially standing waves, whose maximum and minimum sound pressures are detected by microphones strategically positioned along the tube. The distance and number of microphones vary depending on the specific model of the device. The tube must be long enough to allow the formation of at least one maximum and one minimum pressure at the lowest frequency of interest, while keeping the transverse dimensions within certain limits to avoid distortions at the highest measurable frequency.

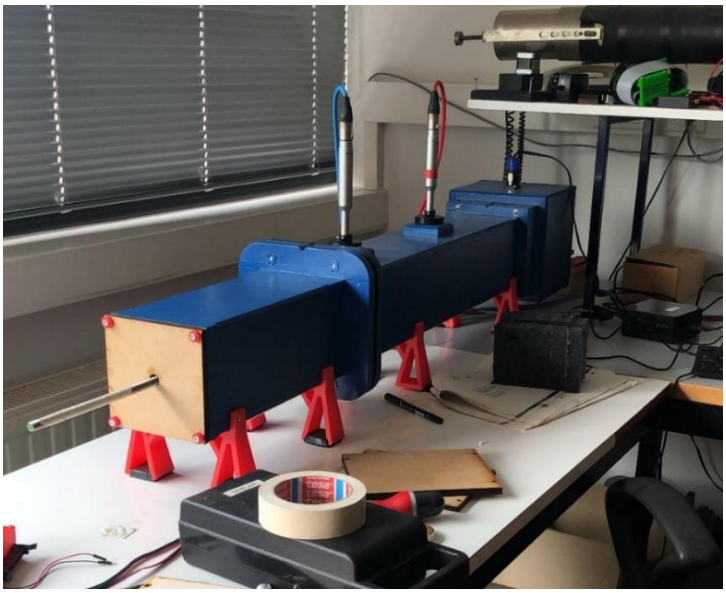

**Figure 8**: An impedance tube at KU Leuven

The use of the impedance tube requires small-sized samples, making it ideal for the development and experimentation of new materials while avoiding the need to create large prototypes for more costly tests in reverberation chambers. This tool, although simple, can be

operated in non-specialized environments, offering flexibility and practicality. However, it's important to note that the results obtained might not fully reflect the behavior of larger samples, limiting the applicability of the method primarily to porous absorbing materials.

Standard configurations require a loudspeaker to generate plane sound waves that, reflecting off the sample, create standing waves useful for calculating both the absorption and the impedance of the material. Cox and D'Antonio [22] describe various measurement methodologies and geometric principles, whose international standardization [77, 78] ensures the reliability and reproducibility of results. The design of the tube should include measures to minimize losses, maintain a constant cross-section, and prevent the formation of transverse modes and resonances. The maximum measurable frequency is determined by the size of the tube and the speed of sound, suggesting the use of tubes of different sizes to cover a wide range of frequencies. The use of multiple microphones can further extend the measurement range, increasing the accuracy and effectiveness of the method.

The accuracy of the measurement depends on the correct cutting and mounting of the sample in the tube, sealing any gaps to avoid overestimations. Materials like petroleum jelly or putty are recommended for an effective seal. The sample should be slightly smaller than the diameter of the tube to avoid mechanical alterations that could affect the measurements. Proper termination of the absorber's back is also crucial to avoid excessive absorption measurements.

# 2 Metodology

The efficacy of HRs in manipulating low frequencies and related research has been extensively documented before, and this thesis is rooted in that context. The starting point for this work is provided by David Jun's research on weakly damped HRs [21]. Throughout his experiments, Jun focused in particular on the capabilities and limitations of HRs when they are devoid of internal sound-absorbing material, identifying a phenomenon that has so far been little explored and understood: modal splitting.

In some simulations [21], Jun observed that the application of an undamped Helmholtz resonator as a surface impedance boundary condition led to the emergence of new modes. The appearance of two side peaks at frequencies slightly lower and higher than the main resonance frequency could be linked to the complex reflection factor. The added modes do not relate to the original dimensions of the room, and this splitting phenomenon could thus be used to lower the Schroeder frequency without sacrificing reverberation time. The emergence of these peaks raises significant questions regarding room-resonator interaction.

The phenomenon of modal splitting is not only of substantial theoretical interest but also raises practical questions related to the design and use of HRs in real acoustic environments. The ability to predict, control or even exploit this effect in an advantageous way could prove important in the context of the acoustic treatment of spaces, expanding the possibilities for intervention on specific frequencies and on the behavior of sound.

This discovery has stimulated the in-depth exploration and experimentation that form the core of this thesis. Through a methodology that integrates simulations and rigorous experimental measurements, it aims to further explore the phenomenon of modal splitting in weakly damped HRs, with the goal of fully understanding its causes, dynamics, and practical implications. It also intends to experimentally explore and validate the differences between the effects of a real resonator and a theoretical one, while also confirming a previously identified modal splitting phenomenon observed in simulations. This dual focus seeks not only to confirm or refute the findings by Jun but also to expand our understanding of these phenomena, paving the way for new applications and design strategies in the field of acoustic engineering.

## *2.1 Choice of environment*

As extensively highlighted in Chapter 1, the characteristics of the environment in which an acoustic experiment takes place are crucial, as they significantly influence sound propagation and the accuracy of results. The preliminary phase of the experiment focuses on selecting the most suitable environment for acoustic measurements. HRs will be designed and calibrated to match the specific acoustic characteristics of this environment. This selection is not a mere detail but plays a fundamental role and presents several challenges.

Identifying the right environment for acoustic experiments requires evaluating various criteria, including the room's geometry and size, its acoustic isolation, and the construction materials' characteristics. The chosen environment has to have parallel surfaces and has to be small enough to have a high Schroeder frequency. Moreover, ensuring effective isolation from external noises is essential to maintain sound purity in the room, avoiding interference from background noises such as traffic or nearby activities.

After carefully evaluating the above criteria, the choice falls on one of the 'transmission rooms' at the KU Leuven acoustics laboratory, a room with semi-reverberation characteristics. Its compact size and trapezoidal prism shape provides a valid context for studying the influence of HRs on internal acoustics. The choice of this room has significance that goes beyond the experimental phase, extending to the applicability of the results.

## *2.2 Simulation*

Following the choice of environment, simulations and theoretical modal analyses follow. For these simulations, the AMROC software is used, which allows for the calculation of resonance modes and sound pressure distributions within a defined rectangular space, making it possible to precisely identify modal frequencies based on the specific dimensions of the room. This approach will be crucial to verify if the observed resonance frequencies align with those theoretically predicted and to investigate the nature of these frequencies, whether they are axial, tangential, or oblique.

Furthermore, to compare the theoretical behavior of a room with a regular shape to that of a room with an irregular shape, the engineering simulation software Ansys is used. This program can analyze environments with complex geometries, allowing for the identification of their theoretical modes based on a three-dimensional model of the room environment.

In continuation with the study on the theoretical acoustic behavior of the room is the development of a Python simulator to anticipate the behavior of the HR by manipulating four key parameters: the thickness of the perforated panel ($t$), the depth of the cavity ($d$), the repetition distance between holes ($D$), and the radius of the holes ($a$).

### 2.2.1 Modes in rectangular approximated room

As stated before, although the test environment resembles a parallelepiped, it is not perfectly regular. It is common practice to use a simplified model for preliminary use of formulas and acoustic reasoning. AMROC calculates the eigenfrequencies, and thus the distribution of acoustic pressure, by first calculating the eigenvalues according to Kuttruff's method [37], using the following equation:

$$k_{n_x n_y n_z} = \pi \left[ \left(\frac{n_x}{L_x}\right)^2 + \left(\frac{n_y}{L_y}\right)^2 + \left(\frac{n_z}{L_z}\right)^2 \right]^{1/2} \tag{17}$$

where $n_x$, $n_y$, and $n_z$ indicate the numbers of nodal planes perpendicular to the x-axis, the y-axis, and the z-axis, respectively, and $L_x$, $L_y$ and $L_z$ are the lengths of the room. These numbers are non-negative integers as a consequence of the boundary condition:

$$\frac{\mathrm{d}p_1}{\mathrm{d}x} = 0 \quad \text{for } x = 0 \text{ and } x = L_x \tag{18a}$$

$$\frac{\mathrm{d}p_2}{\mathrm{d}y} = 0 \quad \text{for } y = 0 \text{ and } y = L_y \tag{18b}$$

$$\frac{\mathrm{d}p_3}{\mathrm{d}z} = 0 \quad \text{for } z = 0 \text{ and } z = L_z \tag{18c}$$

The acoustic pressure distribution associated with these eigenvalues is simply obtained by multiplication of three cosines, each of which describes the dependence of the pressure on one coordinate:

$$p_{n_x n_y n_z}(x, y, z) = C \cos\left(\frac{n_x \pi x}{L_x}\right) \cos\left(\frac{n_y \pi x}{L_y}\right) \cos\left(\frac{n_z \pi x}{L_z}\right) \tag{19}$$

where $C$ is an arbitrary constant.

The eigenfrequencies corresponding to the eigenvalues of equation (17), which are real because of the special boundary condition, are given by:

$$f_{n_x n_y n_z} = \frac{c}{2\pi} k_{n_x n_y n_z} \tag{20}$$

As shown in equation (17) and (20), the calculation of the resonance frequencies of a rectangular room can be done based on its dimensions. Thus, it is crucial to identify the dimensions that best represent the room's fundamental characteristics to correctly apply formulas and acoustic reasoning. To better represent the fundamental characteristics of the room, a rectangle with dimensions that maintain the equivalent area to that of the original room is chosen. While the room's height remains constant and does not significantly vary at different points, the situation is different concerning the sides. Indeed, side ab of the room measures 3.78 m, bc 5.15 m, cd 4.49 m, and da 5.02 m, with angles of 88°, 99°, 81°, and 92° respectively at vertices a, b, c, and d. The height, however, is approximately 4.16 m. By applying Bretschneider's Theorem, the room's area is calculated to be about 20.88 square meters. To create a simplified model, a rectangle with a length of 5.07 meters, close to the average of the two longer sides, and a width of 4.12 meters, necessary to maintain the equivalent area to that of the irregular room, is chosen. This rectangle of 5.07 meters by 4.12 meters provides an adequate approximation for a simplified geometric analysis of the room (see **Figure 9**).

The concept of a "bounding box" to tightly enclose the quadrilateral was also considered. However, although this solution could have provided slightly more precise measurements, the adopted approach yields a qualitatively similar result with less effort.

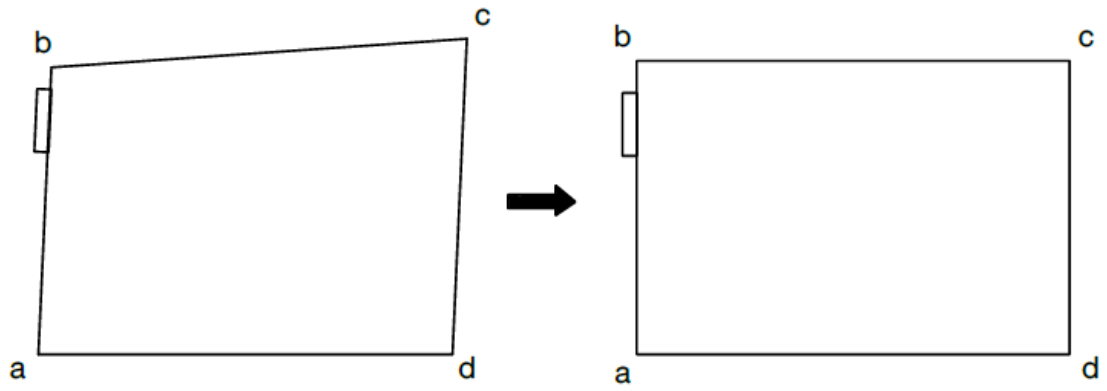


**Figure 9**: Simplified model of the semi-reverberant room

After defining the room's fundamental dimensions, we proceed with the calculation of the theoretical modes and their qualitative classification using AMROC first and Ansys later. Subsequently, for greater clarity, the results will also be expressed through a Python simulator, in which equation (21) for calculating the eigenfrequencies has been implemented. Specifically, in this experiment, the aim is to identify a vertical axial mode, that is, generated between the floor and ceiling and categorized by the triplet 0-0-z. The reason is that in this room, these two surfaces are the only ones truly parallel to each other. This choice will greatly facilitate the management and arrangement of HRs, allowing them to be placed on the ground and easily modify their configuration.

2.2.2 Modes based on numerical simulation carried out in Ansys

For acoustic analysis via Ansys, it is necessary to use a three-dimensional model of the environment under examination. The room analyzed features peculiar geometric irregularities, which extend beyond the non-parallelism of the walls. In particular, it presents a wall with a very

pronounced extrusion. This characteristic is closely connected to the room's specific function: the study of sound transmission between two adjacent spaces.

Once a 3D model that accurately reflects the true dimensions of the room (**see Figure 10**) has been created and imported, ensuring it is devoid of unnecessary details that would burden the software, the first step is to undertake the meshing process.

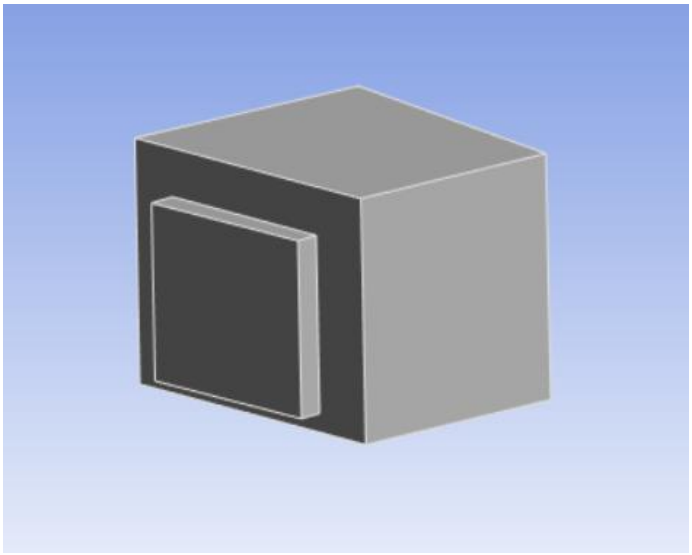

**Figure 10**: Ansys 3D model

This transforms the complex geometry of the model into a network composed of a finite set of elements or cells, thus allowing the execution of numerical simulations. The discretization performed through meshing is fundamental; without it, solving the equations that describe the physics of the environment would be computationally impracticable, given the complexities of the geometries involved. The quality of the mesh directly affects the accuracy of the results: a finer grid ensures a more accurate capture of the acoustic interactions within the environment, although this requires greater computational resources. The definition of the mesh granularity represents a compromise between the search for detail and the limitations of available computational resources.

For the study, the "Modal Acoustics" module is used, which allows identifying the natural vibration modes of the air inside the room, that is, those specific frequencies that induce a particularly intense resonance.

### 2.2.3 Helmholtz resonator performance estimation

In Chapter 1, a general overview of the functioning of HRs was provided, but the equations governing their design have not yet been discussed. These formulas play a crucial role in the development of a Python simulator, which allows for predicting the resonator's behavior by modifying four main parameters. This tool proves essential for virtually testing the effect of different configurations and refining the design before its physical realization, guiding design decisions towards optimizing the acoustic performance of the device.

As previously discussed, by adjusting the depth of the cavity and the size and shape of the holes, it is possible to tune the resonant frequency of the device, achieving maximum absorption precisely at this frequency.

Building on the understanding that adjusting the depth of the cavity and the size and shape of the holes allows for the fine-tuning of the resonator's resonant frequency to achieve optimal absorption, the detailed aspects of the design are explored. An in-depth examination of the physical properties essential for the design and operation of a Helmholtz absorber is conducted.

Among these, the porosity, or fraction of open area, ε, of the perforated sheet that is part of the device, plays a particularly important role. Defined as the ratio of the hole area to the panel cell area, it is described by the equation:

$$\varepsilon = \frac{\pi a^2}{D^2} \tag{21}$$

where $D$ is the repetition distance between holes and $a$ is the radius of the holes.

This quantity allows for the calculation of the device's mass, namely the vibrating air plug inside the holes. However, the effective length of the air plug exceeds the thickness of the perforated panel due to the effect of radiation impedance, which includes the interaction between nearby vibrating air inlets. Therefore, the effective length of the air plug comprises the panel thickness plus end corrections for the radiation impedance of the orifice, requiring the addition of a correction factor $\delta$. Although a standard value for this factor can be set at 0.85, this does not allow for mutual interactions between nearby orifices [22], being based on calculations for a single piston. Consequently, more accurate formulations have been developed, like that of Ingard, applicable when $\varepsilon < 0.16$, described by the equation [6]:

$$\delta = 0.8(1 - 1.4\varepsilon^{1/2}) \tag{22}$$

In the limit of only one hole in an infinite plane, this is roughly 0.85, as given earlier. For a square aperture, this equation changes slightly to [6]:

$$\delta = 0.8(1 - 1.25\varepsilon^{1/2}) \tag{23}$$

An alternative formulation, which works for more open structures and includes the limiting case of $\varepsilon = 1$, was developed by Rschevkin and reported by Cremer and Müller [79]:

$$\delta = 0.8(1 - 1.47\varepsilon^{1/2} + 0.47\varepsilon^{3/2}) \tag{24}$$

With these definitions, it is then possible to calculate the acoustic mass per unit area, expressed as [83]:

$$m = \frac{\rho}{\varepsilon}\left[t + 2\delta a\sqrt{\frac{8v}{\omega}\left(1 + \frac{t}{2a}\right)}\right] \tag{25}$$

where $v$ is the kinematic viscosity of the air, $\rho$ is the density of the air, and $\omega$ is the angular frequency.

At this point, it becomes essential to consider the surface impedance of the resonating system, which is often split into the real term (resistance) and imaginary term (reactance). In general, the real term of surface impedance is associated with energy losses, and the imaginary term with phase changes. So, a simple inspection of the surface acoustic impedance provides more insight into the absorbing properties of a material than the absorption coefficient. However, a proper design method must allow for the determination of both the surface impedance at all frequencies and the absorption coefficient.

The surface impedance of the HR can therefore be expressed through the following relationship:

$$z = r_m + j[\omega m - \rho c \cot(kd)] \tag{26}$$

where $k$ is the wave number in the air; $d$ is the depth of the cavity; $m$ is the acoustic mass per unit area of the panel, and rm represents the resistance term associated with energy losses.
For a Helmholtz device without additional porous absorbent, this term can be calculated using [80]:

$$r_m = \frac{\rho}{\varepsilon}\sqrt{8\nu\omega}\left(1 + \frac{t}{2a}\right) \tag{27}$$

This formulation assumes that the hole radius is not of sub-millimeter dimensions, to ensure that it is larger than the thickness of the boundary layer.

To complete the overall picture, it's necessary to address the last two acoustic quantities that characterize the effect a surface has on an acoustic wave: the pressure reflection coefficient $R$ and the absorption coefficient $\alpha$. If the former, like impedance, provides information about both the magnitude and phase change on reflection, the absorption coefficient does not contain phase data but only gives information about the energy change on reflection.

As mentioned earlier, the pressure reflection coefficient, (sometimes referred to as a reflection factor) indicates the ratio between the reflected and the incident pressure described by equation (11) and its value ranges from -1 to 1. If the surface is completely nonabsorbing, $R = 1$, then the surface pressure is simply double the incident pressure. When the surface is completely absorbing, $R = 0$, then the surface pressure is just the incident pressure. In the case where Z = 0, there is complete absorption; for R equal to -1, there is a completely out-of-phase reflection. In general, for oblique incidences, $R$ can be calculated as follows:

$$R = \frac{\frac{z}{\rho c}\cos(\psi) - 1}{\frac{z}{\rho c}\cos(\psi) + 1} \tag{28}$$

In the case where the incidence angle $\psi$ is normal to the surface, that is $\psi = 0$ degrees, equation (29) can be simplified and brought to the form:

$$R = \frac{z - \rho c}{z + \rho c}, \tag{29}$$

where, $\rho$ is the density of air and $c$ is the speed of sound.

The pressure reflection coefficient $R$ allows the calculation of the absorption coefficient α, as illustrated in equation (12).

Finally, assuming that the sheet thickness $t$ and the hole radius $a$ are much smaller than the wavelength of sound in the air, and that the spacing between $D$ the holes is large relative to the hole diameter, the resonant frequency is:

$$f = \frac{c}{2\pi}\sqrt{\frac{S}{t'V}} \tag{33}$$

where $S = \pi a^2$ is the area of the holes, $t'$ is the thickness of the perforated sheet with the end corrections, and $V$ the volume $= D^2 d$ of each unit cell. This is the same formulation as derived by other methods, such as lumped parameter equivalent electrical circuits [81].

The equations discussed provide a detailed understanding of the fundamental acoustic properties of a HR, offering essential tools for the calculation and analysis of its behavior. The application of these mathematical formulas in the context of simulations emerges as an valuable approach, allowing for a reasonably precise yet simple prediction of the acoustic behavior of the device before its physical realization. The simulator developed with Python for this purpose is designed to be an interactive and intuitive tool: through a user interface that allows dynamic modification of the parameters $t$ (thickness of the perforated panel), $d$ (depth of the cavity), $D$

(repeat distance between the holes), and *a* (radius of the holes), one can immediately visualize the impact of these variations on the absorption coefficient graph. This predictive approach not only facilitates targeted and effective design but also significantly reduces the need for physical experimentation, which can prove to be costly both in terms of time and financial resources.

## *2.3 Experiments*

This section addresses the experimental core of the research. Each procedure and method adopted here not only serves to validate the accumulated theoretical knowledge but also aims to explore the potential and limits of the designed acoustic solutions. The first step, marking the concrete beginning of the project, is the analysis in the semi-reverberant room, a controlled yet challenging environment, whose impulse response is recorded. The goal is to select a specific frequency for tuning the HR, and the most straightforward method for measuring such a device involves tuning to a vertical axial mode, generated between the floor and ceiling.

This fundamental measurement allows us to understand the actual acoustic dynamics of the space and to experiment with the approach that will later be extended to two significantly different environments: the anechoic chamber and the reverberation room.

The section dedicated to the impedance tube, on the other hand, reveals how this instrument is used to measure the surface impedance of samples. It will be seen that this step is crucial in the design of the resonator, as it provides indispensable data for optimizing its acoustic characteristics according to specific needs.

### 2.3.1 Semi-reverberant room

In room acoustics, the room impulse response (RIR) plays a central role, as many acoustic parameters related to the perceived quality of transmission can be derived from it. By transforming the room's impulse response using Fourier transform, the room transfer function is obtained, which can be useful for detecting low-frequency modes. Since the HR in the project must be tuned according to the characteristics of the semi-reverberant room, it is necessary to determine its transfer function. This function describes how an acoustic signal is modified by the environment between the point where it is generated (for example, by a speaker) and the point where it is received (for example, by a microphone), taking into account all the phenomena of reflection, absorption, diffusion, and reverberation that the signal undergoes as it propagates through the room.

In 2001, Muller and Massarani [82] examine the different methods for measuring transfer functions, highlighting how they all share the use of an excitation signal that contains all the frequencies of interest to feed the device under test (DUT). The measurement procedure involves comparing the DUT's response with the original signal. Naturally, there is always a certain amount of noise that reduces the certainty of a measurement. Therefore, it is desirable to use high-energy excitation signals to achieve a sufficient signal-to-noise ratio across the entire range of frequencies of interest.

Muller and Massarani, in their research, highlight how, compared to the use of pseudo-random signals, the measurements of the transfer function using sweeps as the excitation signal show significantly greater immunity against distortions and temporal variances. For example, Maximum Length Sequences (MLS), easily generated and suitable for acquiring impulse responses, are not ideal for all acoustic measurements due to their vulnerability to distortion and temporal variances. Capturing the binaural impulsive responses of a room for high-quality auralization purposes requires a signal-to-noise ratio of >90 dB, difficult to achieve with MLS measurements due to speaker non-linearity but relatively easy to achieve with sweeps, thanks to the possibility of completely rejecting harmonic distortion.

It should also be considered that, due to the wide dynamic range of the human auditory system and the logarithmic relationship between SPL and perceived loudness, any anomaly in the reverberant tail of an RIR is easily recognizable. Using a sweep slightly longer than the RIR to be

recovered allows excluding all harmonic distortion products, leaving practically only background noise as a limitation for achieving the S/N ratio. The sweep can then be fed with considerably more power to the speaker without introducing artifacts into the acquired RIR. Moreover, in anechoic conditions, distortion can be classified into single harmonics relative to the fundamental, allowing simultaneous measurement of the transfer function and frequency-dependent distortion [83, 84].

In light of these considerations, a measurement method based on sweeps is adopted. By using advanced tools like REW (Room EQ Wizard), precise data can be obtained on the frequency response, impulse response, and reverberation characteristics of the room. In addition to the measurement software, which allows analyzing the collected data and interpreting it to understand the acoustic characteristics of the room, other essential tools are required to perform accurate acoustic measurements in an environment.

Firstly, an omnidirectional condenser microphone is used. For these measurements, a DBX DriveRack RTA-M microphone was used, omnidirectional and flat frequency, capable of capturing frequencies between 20 and 20000 Hz. A tripod is essential for placing the microphone in the optimal position and height. Given the modal distribution of sound in the room, it may be necessary to adjust the height of the microphone during different phases of the measurement, while keeping the positions of the source and microphone constant.

Regarding the sound source, a speaker or subwoofer can be used. In acoustically untreated environments, a standard speaker may be sufficient, but for effective capture of low frequencies, the use of one capable of reproducing the lowest frequencies, fundamental for modal analysis of the room, is recommended. For this experiment, the choice fell on a B&K Omnisource 4295 speaker, characterized by omnidirectional broadband acoustic radiation.

The sound card represents a key element in the experiment, acting as an intermediary between the microphone, the measurement software, and the speaker or subwoofer. It is essential that the sound card be equipped with a microphone input with 48V phantom power for the operation of the condenser microphone. Although most sound cards have multiple outputs, for acoustic measurements, it is sufficient to use one to connect the speaker. In this case, the Roland Studio Capture was used.

Finally, the B&K Power Amplifier Type 2716 C is used to effectively adjust the audio signal level from the sound card to the speaker, ensuring that the sound produced is powerful enough to adequately stimulate the room modes. With this tools, several measurements will be conducted in multiple configurations, varying the position the source and the receiver.

To achieve optimal measurements, it is necessary to select the appropriate measurement settings in the dedicated section of REW5. A setting value of 128k corresponds to a sweep length of 2.7 seconds, which is generally adequate for most rooms. However, to have a sweep which is twice the length of the expected impulse respose, the length of the sweep is increased. For each doubling of its duration improves the signal-to-noise ratio by about 3 dB. Therefore, we set a sweep of 10.9 seconds, ranging from 50 Hz to 1000 Hz, as shown in **Figure 11**. This frequency range was chosen as we are not interested in very low frequencies, below 50 Hz, nor in medium-high frequencies, which do not exhibit relevant behaviors to analyze in the context of our study.

Before proceeding with the actual measurement, it is essential to check the signal levels to prevent clipping and to have a reasonable dynamic range of the measurement. At the same time, the signal should not be too weak, as the goal is to observe the decay of sound in space. In environments with a certain level of background noise, it may be advantageous to set a sweep at a relatively high level. Once everything has been correctly set up and verified, the actual acoustic measurement can proceed. The position of the sound source affects the stimulation of different modes; in some cases, certain modes might not be stimulated at all. Similarly, the position of the microphone has a significant impact on the modes detected. If positioned at a node of the modal frequency, the microphone will perceive maximum energy at that frequency. Conversely, if placed at a point of minimum sound pressure (antinode), the detected energy will be minimal for that frequency but could be maximum for others.

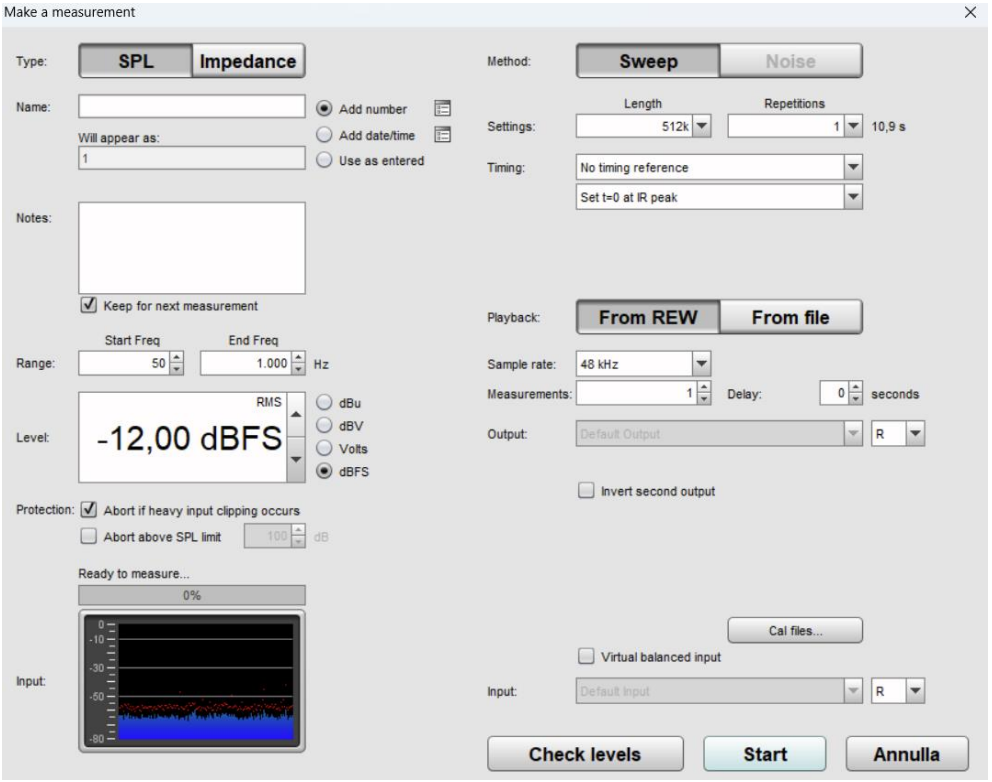


**Figure 11**: REW5 settings for measuraments

To achieve a more detailed characterization of the sound field, multiple measurements are carried out by varying the position of the microphone while keeping the source in its initial position. In position 1, measurements are also conducted at different heights, specifically at 110 cm and 200 cm from the floor. In positions close to the room's boundaries, measurements are made with the microphone pointed towards the corners of the room. The microphone positions during the measurements are qualitatively illustrated in **Figure 12**.

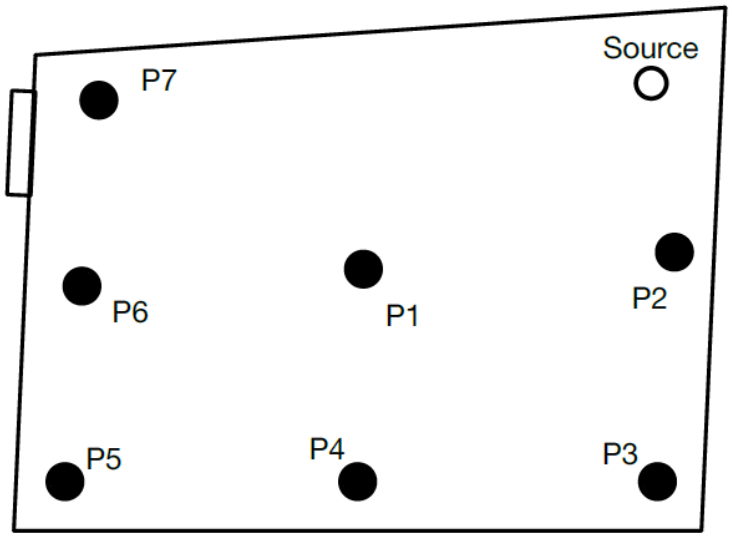


**Figure 12**: Position of the microphone and source in space

**Figure 13** displays the complete setup of the instrumentation in the first configuration, which involves positioning the speaker in a corner of the room and the microphone at the center of the space (position 1), at a distance of 20 cm from the ground.

**Figure 13**: Complete set up of an acoustic measurement

**Figure 14** shows the photograph of the microphone positioned at ground level at the midpoint of a room edge, in positions 2.

**Figure 14**: Microphone positioned in position 2

After conducting a measurement for each microphone position, the analysis of the obtained graphs proceeds to detect frequencies characterized by higher energy concentrations. This process involves a careful comparison between the data collected experimentally and those derived from simulations. Once the mode to be absorbed has been identified, the design of the resonator can proceed.

The return to this room follows the design and tuning of the resonator. In this context, the HRs, which are four identical samples by the end of construction, are strategically placed within the environment. By measuring the room's impulse response again, a comparative analysis is conducted with the measurements taken in the same but empty room. This comparison aims to effectively assess the impact of the resonator on the room's acoustics.

To enhance the experiment's validity, the four resonators are arranged in different configurations, shown qualitatively in **Figure 15**, and their performance is evaluated using various

combinations of microphone and loudspeaker positions. The intention behind all tested configurations is to place the resonators on the floor, thereby maximizing their impact on the targeted vertical mode.

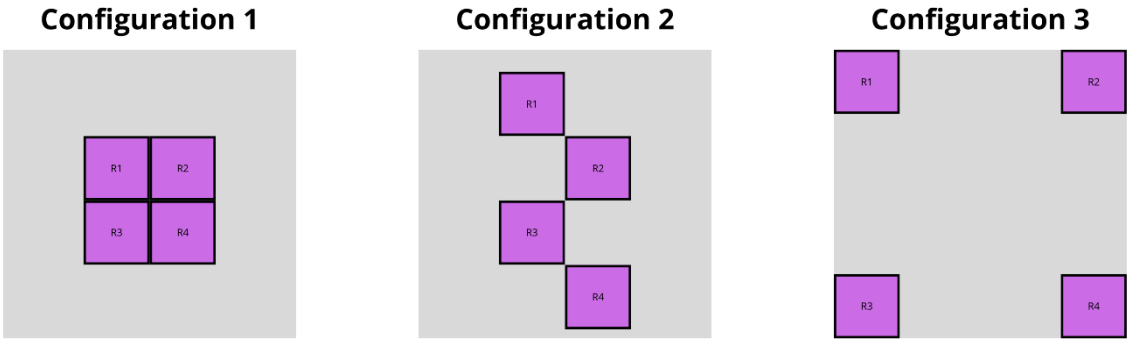


**Figure 15**: Qualitative representation of the three resonator configurations

The first configuration tested involves neatly arranging the four resonators at the center, effectively creating a single large resonator. The second configuration adopts a checkerboard pattern, while the third and final configuration places a resonator in each corner of the room. **Figure 16** shows the microphone and source positions during these measurements. **Figure 17** shows a collection of photos taken during the measurements.

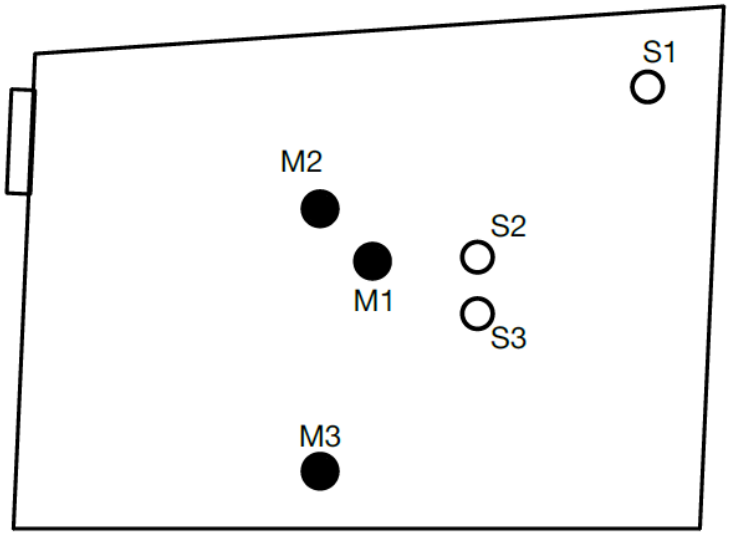


**Figure 16**: Microphone and source positions when testing resonators

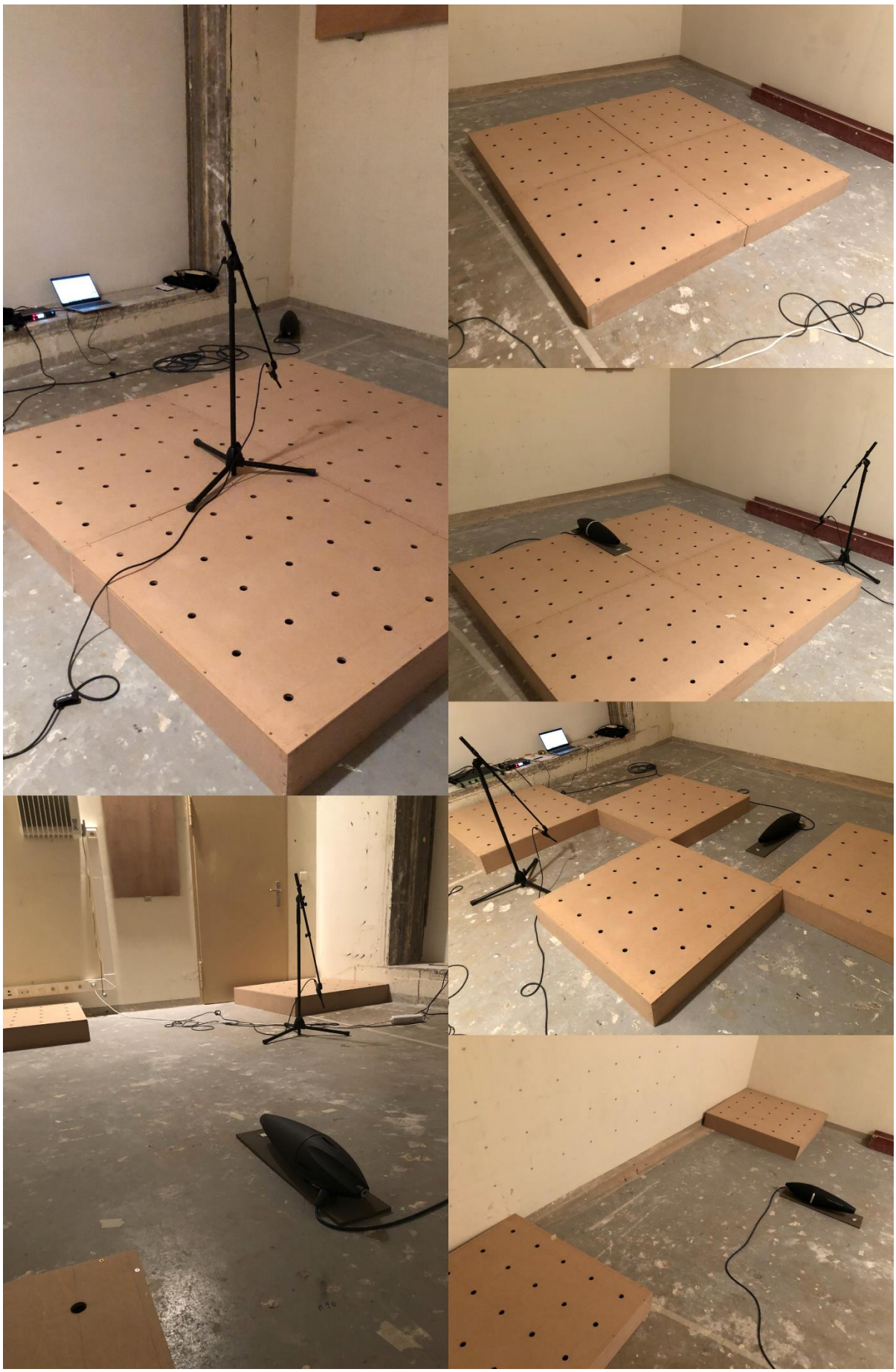

**Figure 17**: Resonators arranged in different configurations

### 2.3.2 Impedance tube measurements

Once the frequency to tune the resonator has been identified, the design and simulation phase established the dimensions of $t$ (thickness of the perforated panel), $D$ (spacing between holes), and $d$ (depth of the cavity). The experiment with the impedance tube is intended to complete the design of the resonator, identifying the optimal value of the parameter $a$ (the radius of the hole). This phase of the project requires an experimental approach, based on empirical and iterative cycles. The production of samples with holes of varying diameters and their evaluation through impedance tube tests are crucial to validate the simulation results.

The impedance tube is an instrument designed to characterize the acoustic properties of a surface at normal incidence over a wide range of frequencies. The standing wave tube method and two-microphone impedance tube method are the most popular experimental procedures for characterizing acoustic absorption.

The latter is nowadays the most used variant and will be the method adopted in this experiment. In the two-microphone impedance tube configuration, the sample to be tested is placed at one end of the tube, while at the opposite end, a loudspeaker is tasked with emitting a sweep. This loudspeaker produces a sound that travels through the tube, forming a planar standing wave. Two pressure measurement microphones, separated by a certain distance $s$ and flush-mounted, are installed between the loudspeaker and the test sample.

Thanks to the use of a digital signal analyzer and dedicated software [85], the complex transfer function is measured between the two microphones and used for pressure reflection coefficient calculation according to following equation:

$$R = \frac{H_{12} - e^{-jks}}{e^{jks} - H_{12}} e^{2jkx_1} \tag{34}$$

where $H_{12}$ represents the transfer function, and $x_1$ indicates the distance from the first microphone to the absorber. This testing method is described by the ISO 10534-2 standard [77, 78], and it is distinguished by its relative complexity but high precision. This technique also allows for the determination of absorption coefficients across a wide range of frequencies in a single session, thus optimizing time and reducing the effort required compared to the older methods, which necessitates the use of a moving microphone and discrete frequency stimulations. For the creation of test samples, MDF panels, made of the same material and thickness as the covering panel of the resonator, were utilized and precisely cut using a laser cutter to ensure maximum accuracy (see **Figure 18**). Each sample features a single hole with a distinct radius, affecting its response to sound.

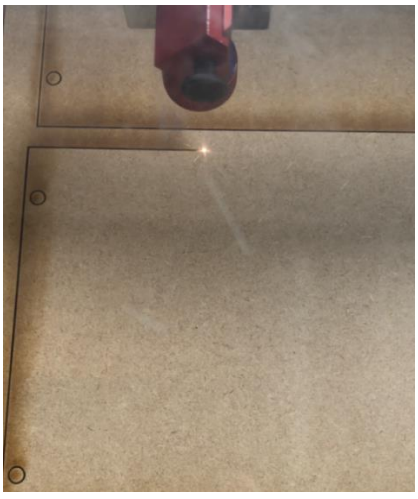

**Figure 18**: A sample being cut by lasercut

A Python script governs the operation of the impedance tube, necessitating its calibration prior to the initiation of measurements to ensure accuracy and reliability. Furthermore, an integrated device systematically measures external temperature, humidity, and atmospheric pressure. These environmental conditions are meticulously considered during the measurement process because they can significantly influence the speed of sound in air, thereby affecting the acoustic measurements. The piston mechanism within the tube allows for the adjustment of the cavity's depth, aligning with the design phase's adjustable depths for the actual resonator.

The aim is to identify samples with optimal surface impedance, indicating their effectiveness in sound absorption. In particular, it is desired that the value of the resistance (the real part of the impedance) be less than 415 to avoid in-phase reflection at the resonance frequency, and that its behavior remains consistent across the entire frequency range of interest, so as to be adjustable for all possible cavity depths.

Tests are conducted for both identical cavities with different samples and varying cavity depths with the same sample. Among the valid *a* values, the one closest to the actual drill bit size used for the resonator's construction was selected. This methodical approach ensures that the resonator's design is based on empirical data, enhancing its acoustic performance. After determining the value of all parameters, it is finally possible to proceed with the physical fabrication of the resonators. First, it was necessary to gather the materials for construction.

### 2.3.3 Anechoic chamber

The experimental validation of the resonators is divided into three phases conducted in three distinct environments: the anechoic chamber, the semi-reverberant room, and the reverberant chamber.

The first experiment studies the behavior of the samples in a dead environment, determining which frequencies are actually absorbed and to what extent, and also aims to verify if the anechoic environment provides the ideal context to isolate the responses of the resonators and refine their tuning. In this context, a single resonator was tested to evaluate its sound absorption capabilities, assuming that consistency among samples would lead to results applicable to all.

Similar to the preliminary acoustic measurements conducted in the semi-reverberant room, the experimental procedure employed a microphone and a speaker, relying on the generation of sound sweeps. An initial measurement was conducted with the empty chamber to provide a baseline for subsequent measurements. During the measurements with the resonator, it was positioned at a distance of 2 meters from the loudspeaker, placed vertically with the sound emitter aligned at the center of the device (see **Figure 19**).

**Figure 19**: A resonator being tested in the anechoic chamber

The microphone, positioned between the sound source and the resonator, was set at the optimal distance of 70 cm, chosen to be small enough to capture a sufficient range of frequencies, yet large enough not to be influenced by the local behaviors of the resonator. This is done to avoid destructive interference around the expected Helmholtz resonance frequency.

Measurements are made by varying the depth of the resonator cavity from 60 to 120 mm, with intervals of 10 mm. When the cavity reaches a depth of 120 mm, the resonator is covered with a rigid and smooth panel (see **Figure 20**). By calculating the ratio between the resonator's response and this last measurement, the speaker frequency response is partially eliminated, and the resulting spectrum shows the difference between Helmholtz and near-to ideal reflection.

The total pressure recorded is given by the sum of the direct incident pressure and the reflection generated by the resonator and can be expressed as:

$$p_{tot} = p_i + p_r \tag{35}$$

with

$$p_i = e^{jkL} \tag{36}$$

and

$$p_r = re^{jkL}e^{jk2x} \tag{37}$$

where $k$ is the wave number, $L$ is the distance from the microphone to the source, and $x$ is the distance from the microphone to the sample.

**Figure 20**: Test of the response of the rigid panel

2.3.4 Reverberation room

After completing the measurements in the semi-reverberant room, the study progresses to the final measurements in the reverberation room, thus completing the examination of the device's functionality. In these measurements, the four resonators are positioned in their configuration as a single unit, as shown in **Figure 21**.

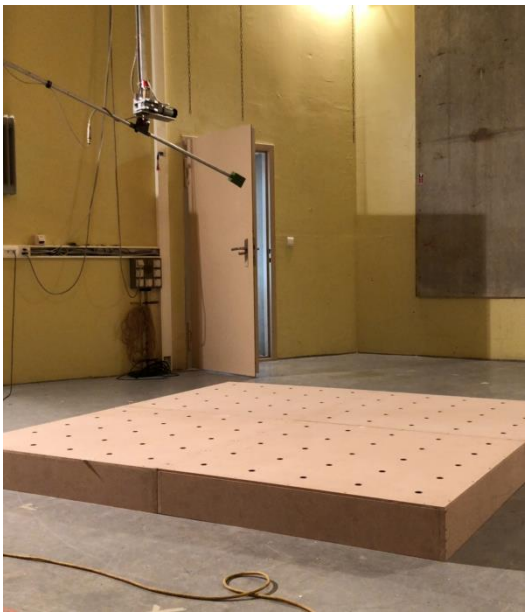

**Figure 21**: Measurement in the reverberation chamber

In this configuration, the sound sources are already positioned in the corners of the room, and the measurements must be managed from the control room. The command to start the measurements is given from the control room, and at the end of each measurement, an automatic system moves the microphone, which is mounted on a suspended scaffolding, changing its position. The positions of the microphone and the sources are qualitatively shown in **Figure 22**.

These measurements are crucial as they are the only method to properly showcase the absorption characteristics of the resonator, through the difference in reverberation times. According to ISO 354 standard, the reverberation time of the room in the frequency band is calculated through the arithmetic mean of the total number of reverberation time measurements in the frequency band. Once the reverberation times in one-third octave bands are calculated, the following formulas lead to the calculation of the absorption coefficient:

$$A_1 = \frac{55.3V}{cT_1}, \tag{38}$$

$$A_2 = \frac{55.3V}{cT_2}, \tag{39}$$

$$A_T = A_2 - A_1, \tag{40}$$

$$\alpha_S = \frac{A_T}{S}, \tag{41}$$

where, $T_1$ is the reverberation time of the empty room, $T_2$ is the reverberation time with the sample inside, c is the speed of sound, $V$ is the volume of the room, $A_1$ is the equivalent

absorption area of the empty room, $A_2$ is the equivalent absorption area of the room with the sample inside, and $A_t$ is the equivalent absorption area of the sample. The absorption coefficient is finally calculated as the ratio between $A_t$ and $S$, which is the area covered by the sample, in square meters.

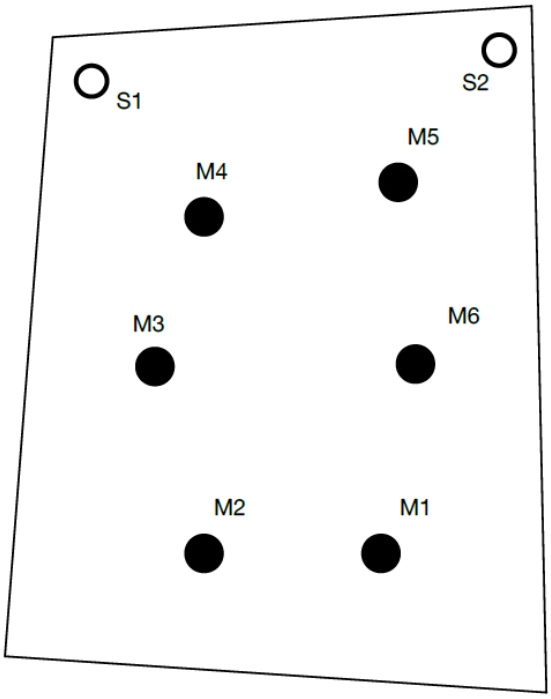


**Figure 22**: Qualitative position of microphones in the reverberant chamber

# 3 Results

The previous chapter outlined the methodology used to conduct the experiments and simulations, laying the groundwork for understanding the effectiveness of HRs in manipulating low frequencies. Following this methodological foundation, Chapter 3 is dedicated to the detailed presentation of the results emerged from the experimental approach and is structured into three key sections that reflect the sequential progression of the work: the analysis of the test environment, the design of the HR, and the experiments conducted in various environments with the HRs. Each section presents the results in a clear and systematic manner, thus ensuring a cohesive and easily navigable narrative.

## *3.1 Semi-reverberant room*

Having defined the fundamental dimensions of the test room allowed to calculate the theoretical modes and their qualitative classification with AMROC software. Being primarily a program for the analysis of room acoustics at low frequencies, AMROC by default shows the resonance frequencies in the range between 30 and 200 Hz (see **Figure 23**).

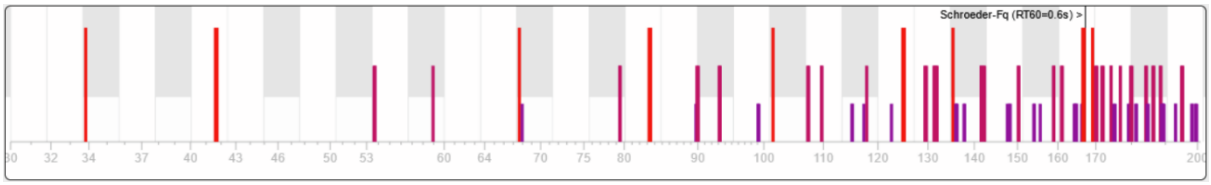


**Figure 23**: Room modes calculated by AMROC

Among those represented, our analysis focuses on the vertical axial modes, as they are the ones truly important for the experiment. As mentioned earlier, the modes are identified by the triplet x-y-z, where each number represents the number of half wavelengths along the room's dimensions. The vertical axial modes, identified as 0-0-z, occur along the height of the room, while the horizontal axial modes, identified as x-0-0 or 0-y-0, manifest along the length and width. Each mode can have higher harmonics, which are multiples of its fundamental frequencies. These harmonics appear when sound waves reflect multiple times between the walls, creating more complex sound pressure patterns.

AMROC provides, represents, and explains these mode details through a detailed table that lists the identified modes in the room, indicating frequency, musical note, modal configuration (x-y-z), and type (axial, tangential, or oblique). **Figure 24** shows the energy distribution of the vertical axial modes up to the one identified by the triple 0-0-3.

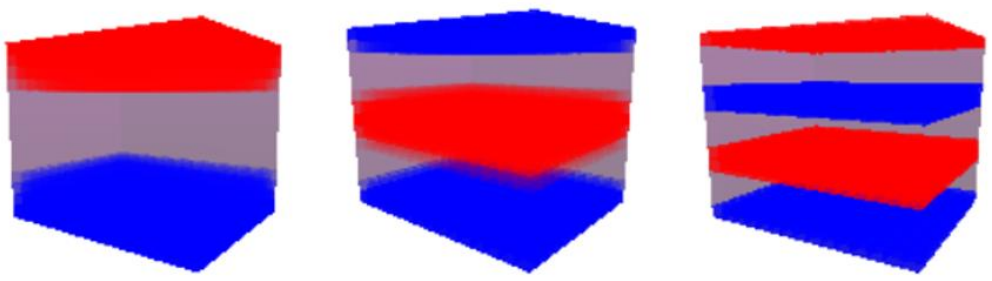

**Figure 24**: Energy distribution of the vertical axial modes

**Table 1** shows the top 43 modes. This detailed representation allows us to associate a theoretical mode to the resonance frequencies detected through experimental measurements and to understand their energy distribution in space. In the comprehensive analysis of acoustic modes within the test environment, **Table 2** presents a dataset derived from computational simulations conducted using Ansys.

**Table 1**: Theoreticals modes calculated by AMROC

| Mode number | Frequency | Musical note | Triple | Type |
|---|---|---|---|---|
| 1 | 33.83 Hz | C1# | 1-0-0 | ax |
| 2 | 41.23 Hz | E1 | 0-0-1 | ax |
| 3 | 41.63 Hz | E1 | 0-1-0 | ax |
| 4 | 53.33 Hz | G1# | 1-0-1 | tan |
| 5 | 53.64 Hz | A1 | 1-1-0 | tan |
| 6 | 58.59 Hz | A1# | 0-1-1 | tan |
| 7 | 67.65 Hz | C2# | 1-1-1 | obl |
| 8 | 67.65 Hz | C2# | 2-0-0 | ax |
| 9 | 79.22 Hz | D2# | 2-0-1 | tan |
| 10 | 79.43 Hz | D2# | 2-1-0 | tan |
| 11 | 82.45 Hz | E2 | 0-0-2 | ax |
| 12 | 83.25 Hz | E2 | 0-2-0 | ax |
| 13 | 89.12 Hz | F2 | 1-0-2 | tan |
| 14 | 89.49 Hz | F2 | 2-1-1 | obl |
| 15 | 89.86 Hz | F2 | 1-2-0 | tan |
| 16 | 92.36 Hz | F2# | 0-1-2 | tan |
| 17 | 92.9 Hz | F2# | 0-2-1 | tan |
| 18 | 98.36 Hz | G2 | 1-1-2 | obl |
| 19 | 98.87 Hz | G2 | 1-2-1 | obl |
| 20 | 101.48 Hz | G2# | 3-0-0 | ax |
| 21 | 106.65 Hz | G2# | 2-0-2 | tan |
| 22 | 107.27 Hz | A2 | 2-2-0 | tan |
| 23 | 109.53 Hz | A2 | 3-0-1 | tan |
| 24 | 109.68 Hz | A2 | 3-1-0 | tan |
| 25 | 114.49 Hz | A2# | 2-1-2 | obl |
| 26 | 114.92 Hz | A2# | 2-2-1 | obl |
| 27 | 117.17 Hz | A2# | 0-2-2 | tan |
| 28 | 117.18 Hz | A2# | 3-1-1 | obl |
| 29 | 121.96 Hz | B2 | 1-2-2 | obl |
| 30 | 123.68 Hz | B2 | 0-0-3 | ax |
| 31 | 124.88 Hz | B2 | 0-3-0 | ax |
| 32 | 128.22 Hz | C3 | 1-0-3 | tan |
| 33 | 129.38 Hz | C3 | 1-3-0 | tan |
| 34 | 130.5 Hz | C3 | 0-1-3 | tan |
| 35 | 130.75 Hz | C3 | 3-0-2 | tan |
| 36 | 131.26 Hz | C3 | 3-2-0 | tan |
| 37 | 131.51 Hz | C3 | 0-3-1 | tan |
| 38 | 134.81 Hz | C3# | 1-1-3 | obl |
| 39 | 135.3 Hz | C3# | 2-2-2 | obl |
| 40 | 135.31 Hz | C3# | 4-0-0 | ax |
| 41 | 135.79 Hz | C3# | 1-3-1 | obl |
| 42 | 137.22 Hz | C3# | 3-1-2 | obl |
| 43 | 137.58 Hz | C3# | 3-2-1 | obl |

**Table 2**: Theoretical modes by Ansys

| Mode number | Frequency |
|---|---|
| 1 | 34,585 |
| 2 | 39,565 |
| 3 | 42,684 |
| 4 | 54,373 |
| 5 | 54,666 |
| 6 | 59,118 |
| 7 | 68,131 |
| 8 | 69,256 |
| 9 | 76,171 |
| 10 | 80,451 |
| 11 | 80,671 |
| 12 | 84,858 |
| 13 | 89,503 |
| 14 | 89,860 |
| 15 | 91,119 |
| 16 | 91,614 |
| 17 | 94,187 |
| 18 | 99,818 |
| 19 | 100,59 |
| 20 | 102,06 |
| 21 | 105,95 |
| 22 | 108,59 |
| 23 | 109,59 |
| 24 | 110,29 |
| 25 | 113,65 |
| 26 | 114,94 |
| 27 | 117,16 |
| 28 | 118,04 |
| 29 | 119,10 |
| 30 | 123,46 |
| 31 | 123,75 |
| 32 | 127,78 |
| 33 | 128,01 |
| 34 | 130,87 |
| 35 | 131,67 |
| 36 | 132,94 |
| 37 | 133,69 |
| 38 | 134,27 |
| 39 | 135,46 |
| 40 | 137,68 |
| 41 | 139,24 |
| 42 | 139,96 |
| 43 | 140,75 |

Within the semi-reverberant room, a total of 9 preliminary measurements are conducted, keeping the source always in the same position and moving the source between positions 1 and 7 as depicted in **Figure 12**.

The **Figure 25** displays the Room Impulse Responses (RIRs) for the test initially conducted at heights of 20, 110, and 200 cm, respectively. From this point forward, measurements conducted at the height of 20 cm will be referred to as "ground level" measurements.

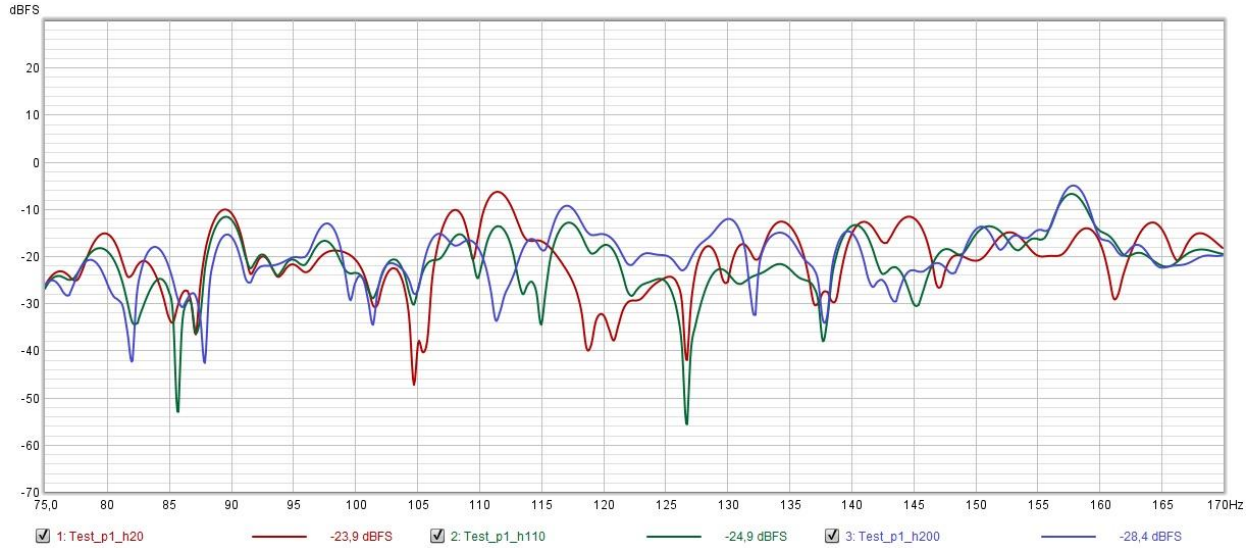


**Figure 25**: RIRs of the semi-reverberant room for the measurements taken at position 1

The SPL and Phase graph displays frequency and phase responses. Frequency responses are labeled with the measurement name, and phase responses are depicted with a dashed line on the graph's right Y-axis. To obtain accurate phase information, it is crucial to eliminate any time delay from the Impulse Response, as it causes a phase shift that increases with frequency, ensuring that the position is zero on the time axis. **Figure 26** provides an example of the phase graph, however, however there will be no further reference to this graph in the data analysis.

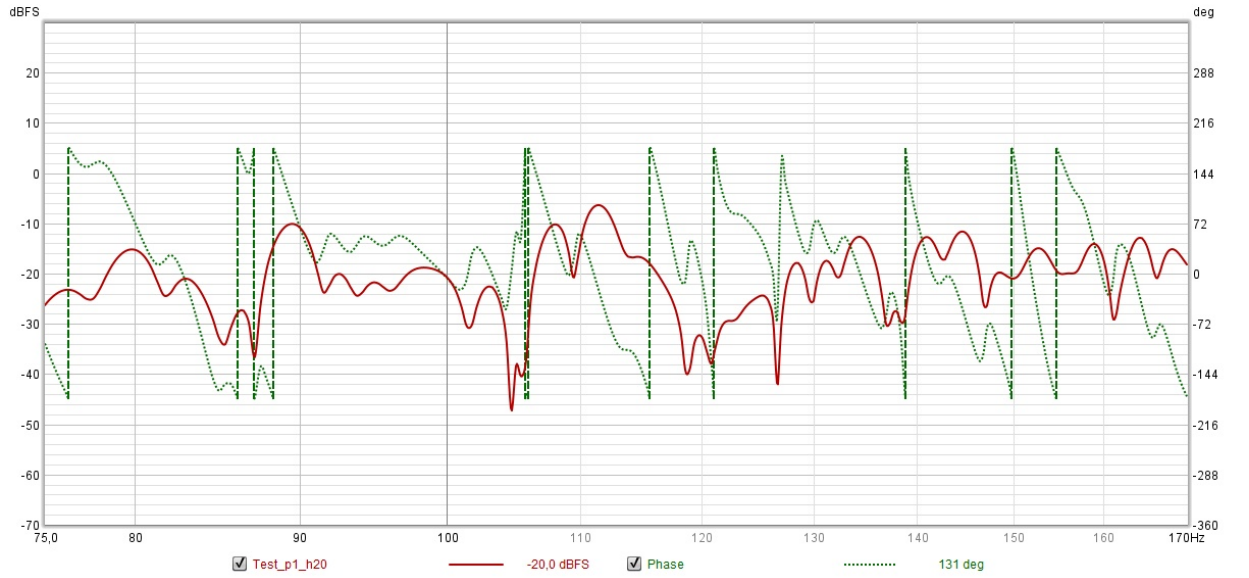


**Figure 26**: Graph of the Sound Pressure Level and phase of a measurement in a semi-reverberant chamber

Subsequent measurements are carried out at the centers of the edges and in the corners of the room, all at ground level, and their RIRs are shown in **Figure 27.**

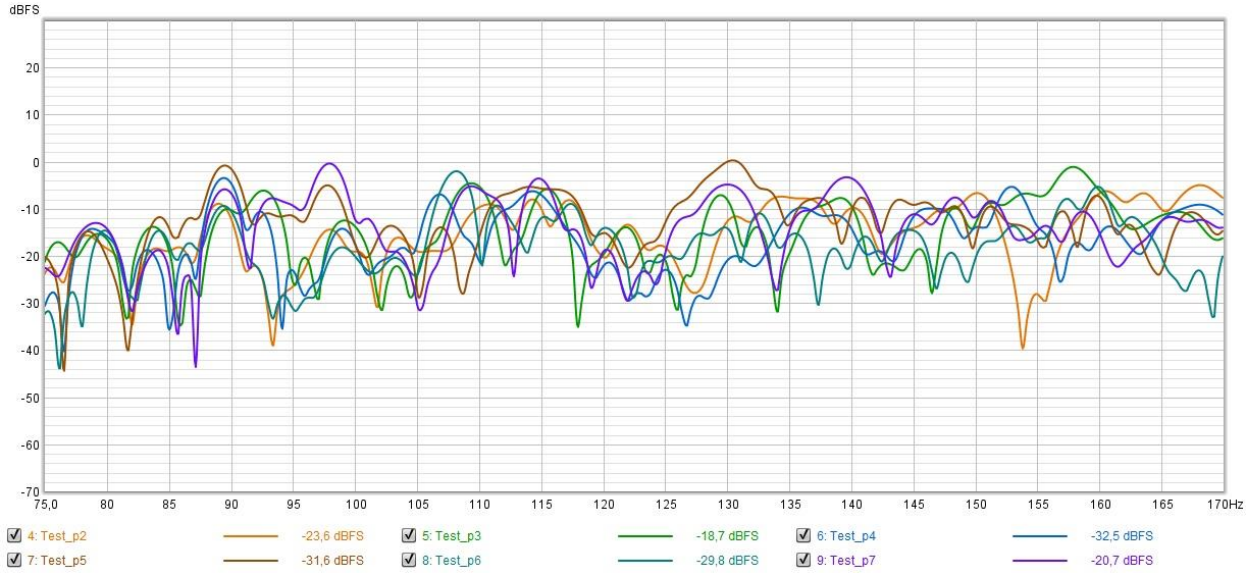


**Figure 27**: RIRs of the semi-reverberant room for the measurements taken at positions 2-7

To further explore and gain a broader understanding of the measurements, the spectrogram, an instrumental tool for analyzing room modes, is consulted. The spectrogram is a type of time-frequency graph that illustrates how frequency content changes over time, proving especially useful for examining results from sweep measurements. The intensity of sound is depicted through color. The graph features five modes: Fourier, Wavelet, Airy CWT, Morlet CWT, and Burst Decay. The Fourier mode employs the Short-Term Fourier Transform (STFT). In the Fourier and wavelet modes, when viewing sweep measurements, time starts before the impulse peak to allow observation of the response onset. Regions where the response decays more slowly manifest as streaks along the time axis. A dashed line tracks the peak energy time, indicating the peak level across the graph for each frequency. This can spotlight variations in the arrival of peak energy across frequencies—an ideal peak energy time trace would be a straight line, maintaining the same time value across all frequencies. The graph utilizes logarithmically spaced data at 96 points per octave, facilitating a detailed and dynamic representation of acoustic behavior. **Figure 28** displays the spectrogram of the measurement taken at position 1 at ground level.

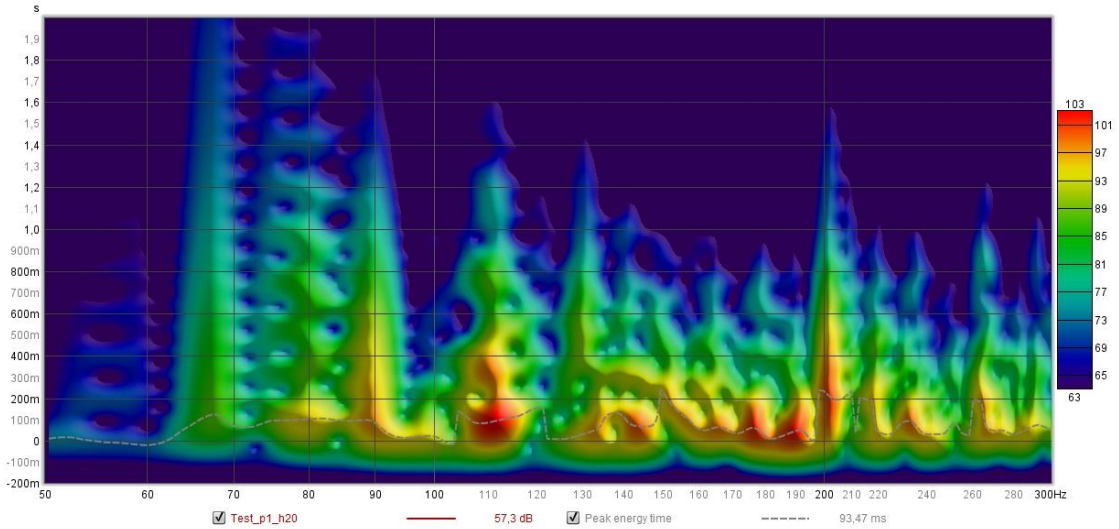


**Figure 28**: Spectrogram of a measurement in a semi-reverberant chamber

To achieve an even more accurate and intuitive graphical representation, an additional tool is used: a simulator developed in Python. This in-house created software processes the data obtained through REW5, displaying it graphically with red vertical markings indicating the theoretical modal frequencies calculated with simulations. These calculations are based on the fundamental dimensions of the room and calculate modes according to Kuttruff [37]. By taking measurement 1 as an example, this methodology allows for a direct comparison between the theoretically predicted modes for the room and those observed (see **Figure 29**).

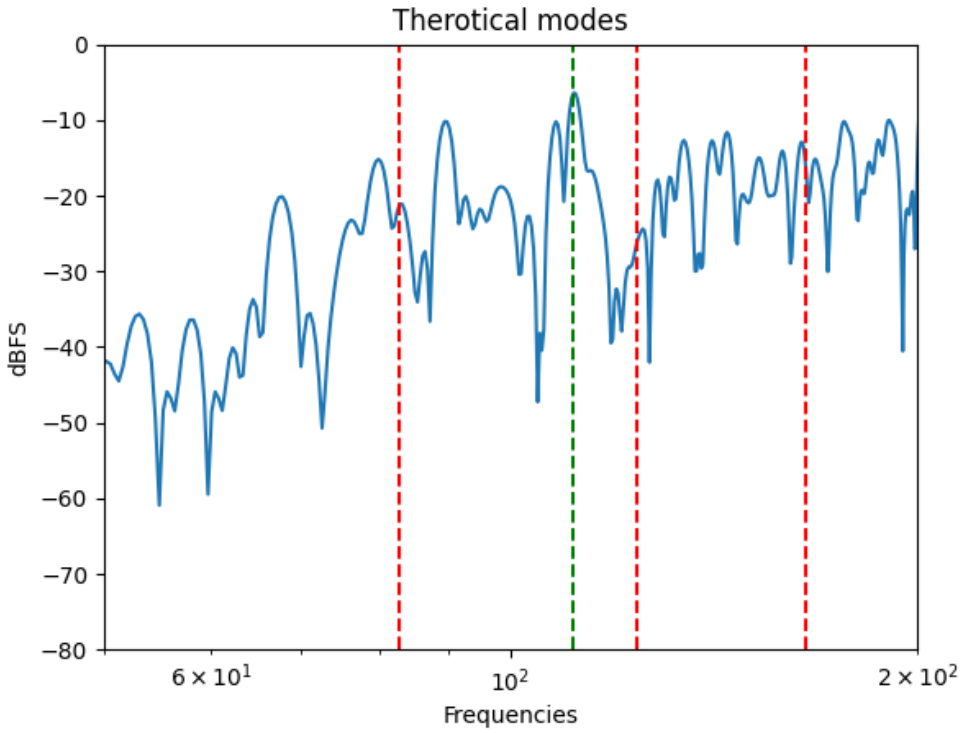


**Figure 29**: Theoretical modes calculated according to Kuttruff overlaid on the Room Impulse Response

The theoretical modes calculated for a rectangular geometry must be compared with the theoretical modes revealed by ANSYS through the finite element method and reported in the **Table 3**.

The analysis of preliminary data leads to the choice of a target frequency to which to tune the weakly damped HR. After the completion of the resonator, new measurements are taken, adapting the position of the source and microphone to the resonator configurations.

**Figure 30** depicts the graph of sound pressure levels of the empty room and the room with the resonators inside, for the measurement conducted in the position with the resonators in configuration 1, the source at position s1, and the microphone at position m1 at ground level. Additionally, the respective transfer function is shown, which is the ratio between the sound pressure influenced by the resonator and the reference sound pressure.

**Figure 31** illustrates the average of the mean sound pressures for measurements taken at ground level and the corresponding transfer function.

In **Figure 32**, the transfer functions of configurations 1, 2, and 3 are compared.

In **Figure 33**, the difference between the transfer function of the mean measurements and the measurements taken with the source at position s2 and the microphones at positions m1 and m2 is observed.

Finally, **Figure 34** shows the transfer functions for configuration 3, measured in the case of four resonators arranged in the corners or in the case of using only three resonators. The latter measurement was made to be able to exit the room during the measurement.

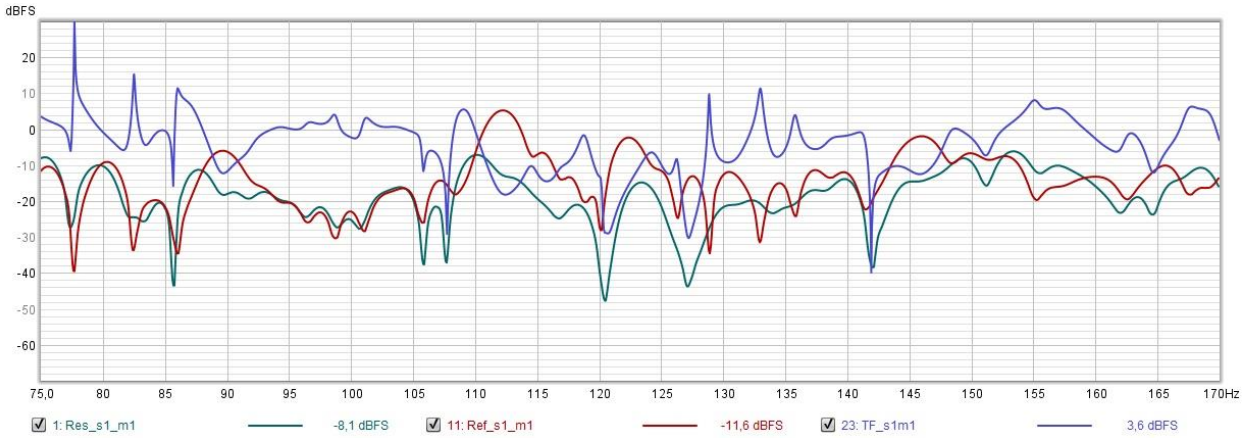


**Figure 30**: Sound pressure levels for configuration 1, positions s1 and m1, and TF

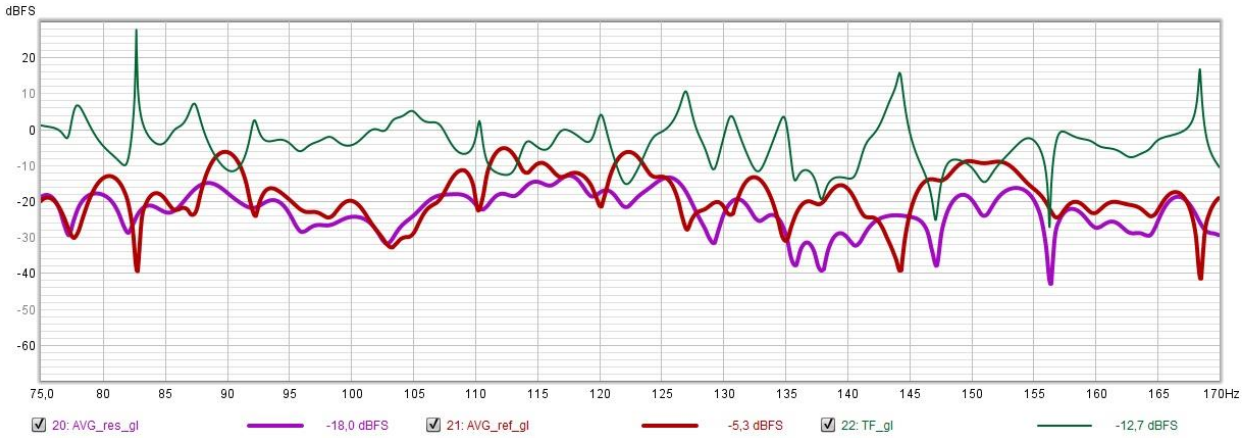


**Figure 31**: Average sound pressure levels at ground level and TF

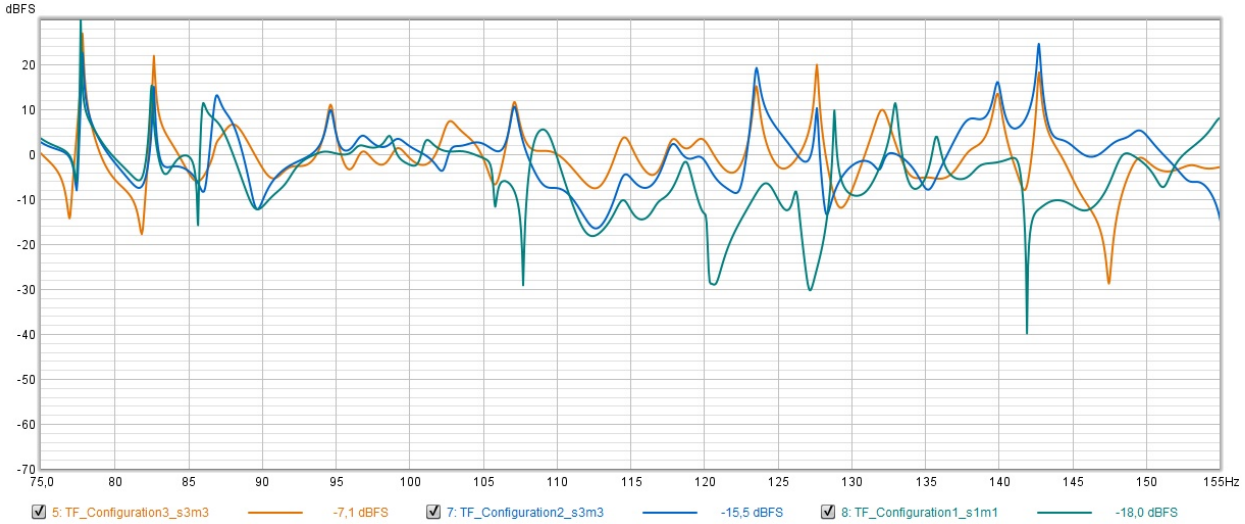


**Figure 32**: Comparison among the transfer functions of the 3 configurations

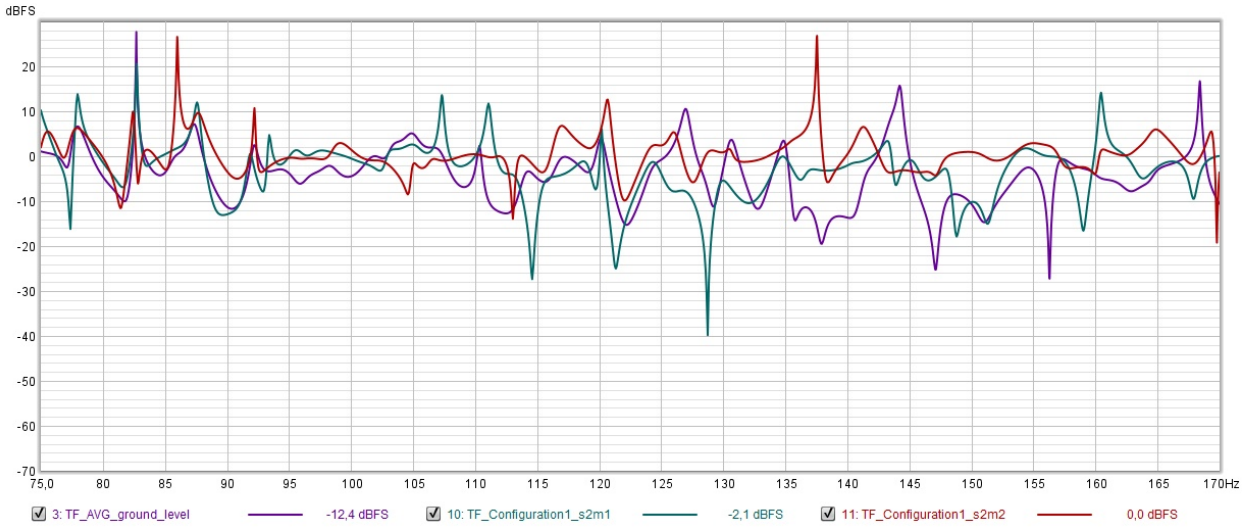


**Figure 33**: Transfer functions for configuration 2 compared with average transfer function of the measurements taken at ground level

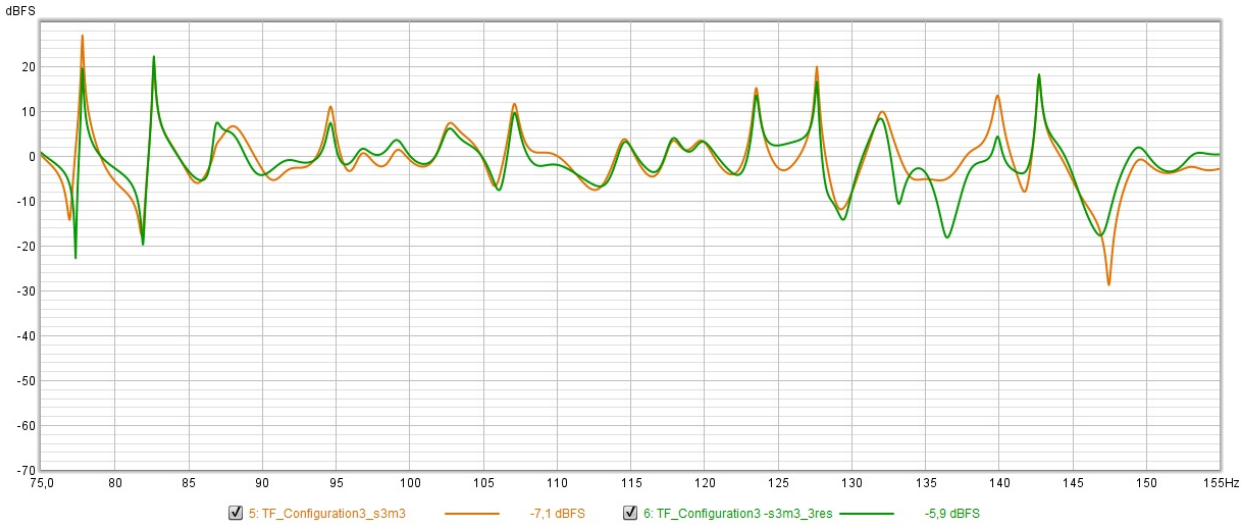


**Figure 34**: Transfer functions for configuration 3

## *3.2 Resonator design*

Subsequently, all the equations discussed are integrated into a Python simulator for calculating the resonance frequency of the resonator and, concurrently, the amplitude and shape of the absorption curve associated with the resonance peak.

As can be observed from **Figure 35**, the graph illustrates the absorption coefficient for the default configuration of parameters t, d, D, and a. Through the simple and intuitive interface, shown in **Figure 36**, it is possible to dynamically change these values, obtaining a real-time update of the graph.

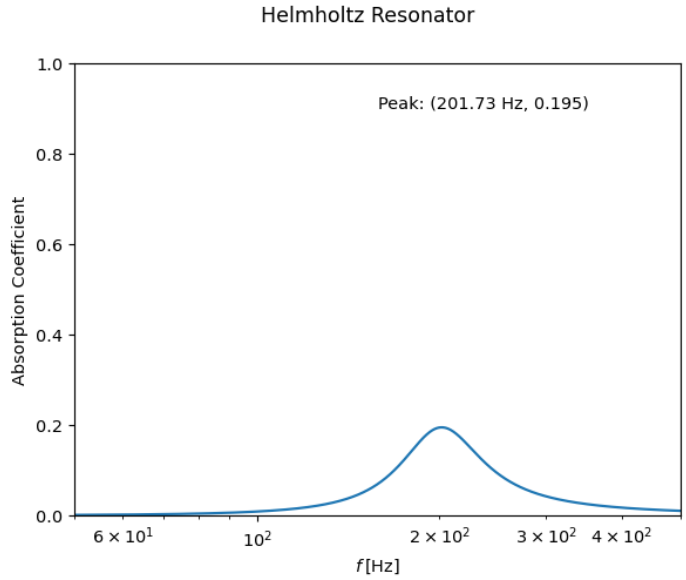


**Figure 35**: Graph of the absorption coefficient of the simulated resonator


**Figure 36**: User interface with default parameter values

The amplitude and height of the parabola are associated with the bandwidth extension and the maximum absorption level that the resonator can provide at the resonance frequency. By varying the four mentioned parameters, it is possible to configure the resonator to absorb the same frequency with different bandwidth and absorption characteristics. A wide curve with a less pronounced peak indicates extended absorption over a broader frequency band but with a lower maximum absorption level for each frequency. Conversely, a tighter and more pronounced curve suggests greater absorption but focused on a more limited frequency range.

Once the initial values of the parameters t and D were defined, the Python simulator is used to draw a preliminary estimate of the absorption coefficient. **Figure 37** illustrates the absorption curve obtained by setting t=9 mm, D=200 mm, with d and a set to the default values of 100 mm and 10 mm, respectively. The simulation allows observing the effects of parameter variations on the frequency response of the device, indicating the need to further refine the values of d (cavity depth) and a (radius of the perforations) to achieve precise tuning.

As previously illustrated, there are multiple configurations that can align the absorption peak with the desired frequency, while respecting the constraints of scientific realism and practical feasibility. Therefore, finding a unique and definitive solution represents a complex challenge.

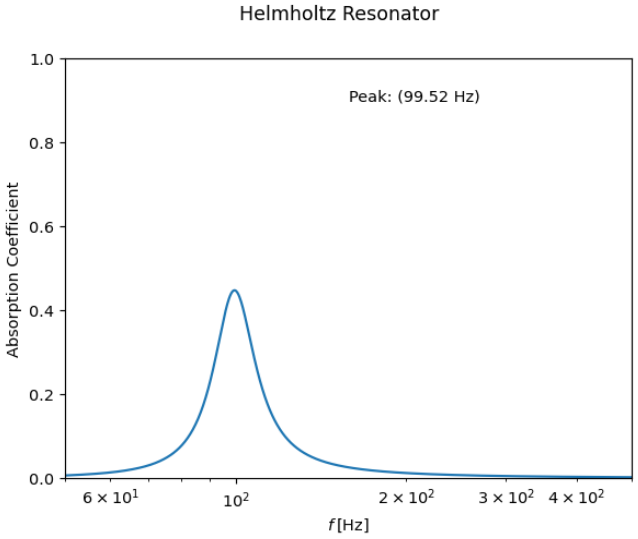


**Figure 37**: Absorption coefficient graph for t = 9 and D = 200

For example, by keeping t and D fixed, different pairs of values for d and a can achieve optimal absorption at 125.86 Hz. The combinations of a=4.80 mm with d=83 mm, a=5.60 mm with d=106.50 mm, a=7.85 mm with d=179.50 mm, and a=8.45 mm with d=200 mm, all result in maximum absorption at the frequency of 125.86 Hz, and clearly, there are other intermediate combinations as well. However, it is observed that the absorption level progressively decreases with increasing values of a and d, with the absorption curve becoming less sharp, indicating a wider absorption band. **Figure 38** represents these examples, visually demonstrating the effect of various configurations on the frequency response of the resonator.

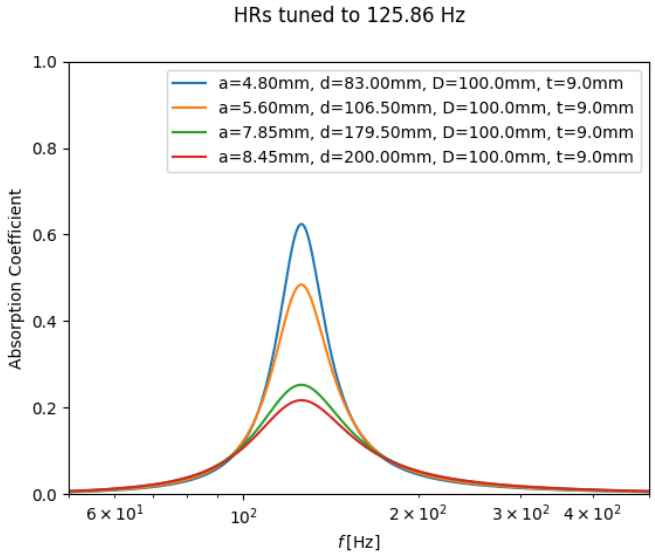


**Figure 38**: Graph of the absorption coefficient with peak at 125.86 Hz for different combinations of a and d

## *3.3 Impedance Tube*

The approach adopted in the impedance tube experiment follows an empirical methodology of trial and error. Within the scope of this study, the parameters *t* and *D* are to be considered

constant at 9 mm and 100 mm, corresponding respectively to the thickness of the samples and the cross-sectional area of the tube. The first sample to be tested is characterized by a hole with a radius of 4 mm and is measured by setting the depth of the tube to 90 mm. **Figure 39** shows the value of the real part of the surface impedance measured for this sample in the frequency range between 60 and 200 Hz. The dashed red lines show the reference values, respectively equal to 0 (green line) and 415 (red line). As previously mentioned, this measurement aims indeed to find an optimal resistance value, between 0 and 415 Rayls across the entire range of potentially interesting frequencies.

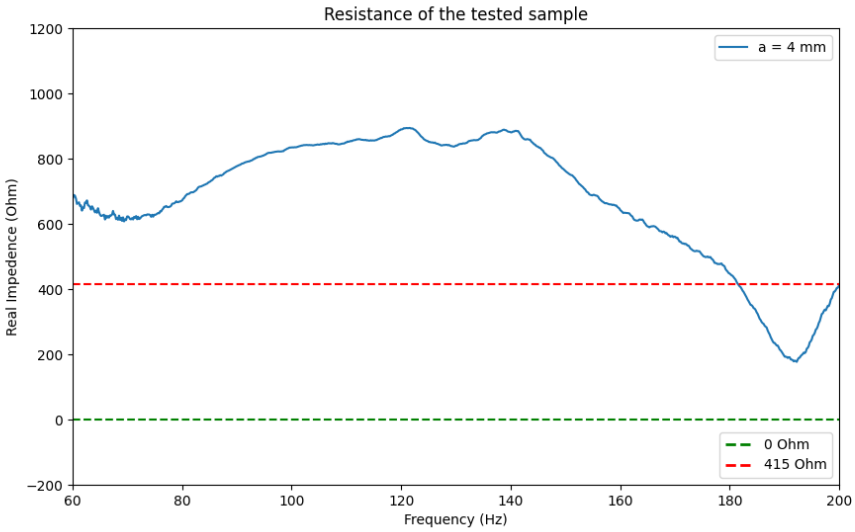


**Figure 39**: Sample resistance with hole radius 4 mm

Subsequently, samples with hole radius of 5, 6, and 7 mm are explored (see **Figure 40**). In the absence of identification of optimal values, the procedure involves gradually increasing the hole diameter up to 20 mm, as shown in the **Figure 41**.

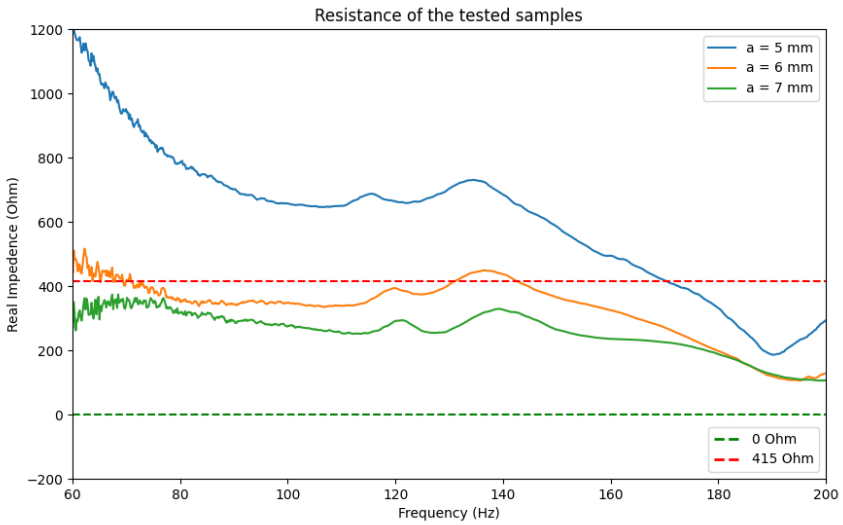


**Figure 40**: Resistance of samples with hole radius 5, 6 and 7 mm

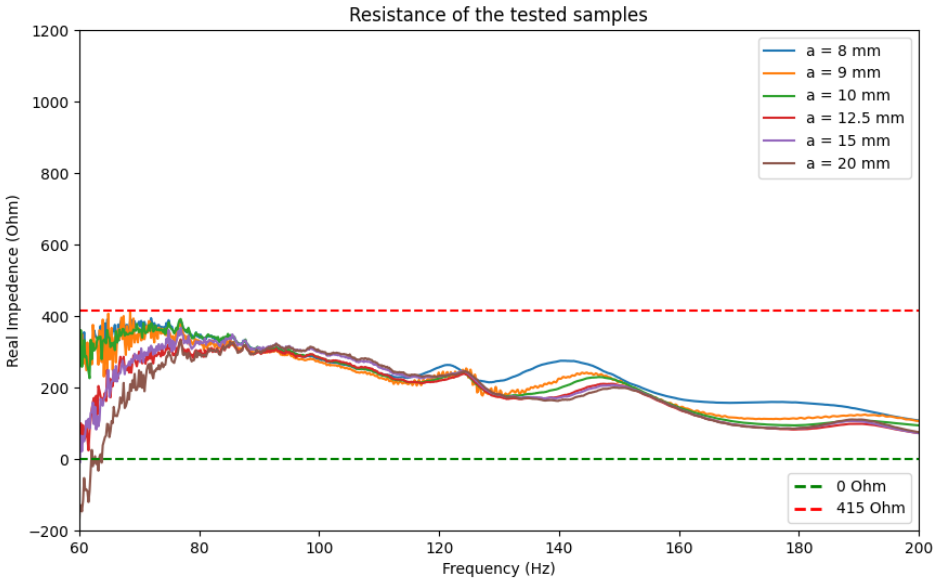


**Figure 41**: Resistance of samples with hole radius 9, 9, 10, 12.5, 15, 20 mm

For each sample, the equivalent HR is calculated using simulation. Then, the expected values of absorption coefficient α, porosity ε, resistance $r_m$, and the product $\varepsilon \circ r_m$ are compared with those obtained experimentally.

Finally, the sample with a hole diameter of 12.5 cm is selected as the definitive model for further experiments. A subsequent series of measurements is conducted, varying the cavity depth to further experimentally confirm that modifying this variable does not impact performance.

## *3.4 Resonator production*

After determining the value of all parameters, it is possible to proceed with the physical fabrication of the resonators. First, it is necessary to gather the materials for construction. To ensure maximum precision cuts, the boards are processed directly at the supplier using specialized equipment (see **Figure 42a**).

Given the need to create a resonator with a one-square-meter base cavity, the overall dimensions of the device are appropriately increased to fit the planned structure. The top panel is sized at 1036 mm on each side, while the sideboards for the perimeter are cut in pairs, two at 1036 mm and two at 1000 mm, all with a height of 150 mm and thickness of 18 mm. This configuration ensures that the internal cavity precisely maintains a one-square-meter base. **Figure b** shows the frame of the resonator under construction.

The assembly of the resonator is entirely hand-done to ensure utmost attention to detail. Despite nominally identical dimensions, slight dimensional differences among the boards are noted, due to variations in the cutting process or handling, requiring careful selection and pairing of boards to ensure the dimensional consistency of the resonator. One of the crucial components, the piston, is made with a panel of dimensions 996x996 mm and thickness of 18 mm, surrounded by a draft excluder tape to ensure airtightness (see **Figure c**). **Figure d** shows the support blocks with a thickness of 12 mm used to support the base of the piston. This arrangement defines a maximum cavity depth of 120 mm, resulting from subtracting the thickness of the support blocks and the piston panel from the total cavity height of 150 mm.

The final stage of the resonator construction involves making holes on the surface panel. To proceed accurately, a grid is first drawn on the surface of the panel. This grid aims to precisely locate the points for drilling, ensuring that the holes are evenly distributed and respect the predetermined distances. Subsequently, a drill equipped with a bit of the specified diameter is used, in line with the design requirements for the resonator.

To maximize the efficiency of the production process, each phase of the resonator construction is carried out in parallel on each of the four units, following a methodology similar to an assembly line. This approach allowed for reduced production times while maintaining a high standard of quality and consistency among the resonators. After assembly and drilling, each resonator is carefully finished, smoothing surfaces to remove any imperfections and rounding edges to ensure a clean and uniform final appearance. At the end of these processes, four aesthetically identical and functionally homogeneous resonators are obtained, although slight dimensional variations attributable to the tolerances of the cutting and assembly processes are inevitably present. **Figures e** and **f** show photographs of a single resonator and four identical ones respectively.

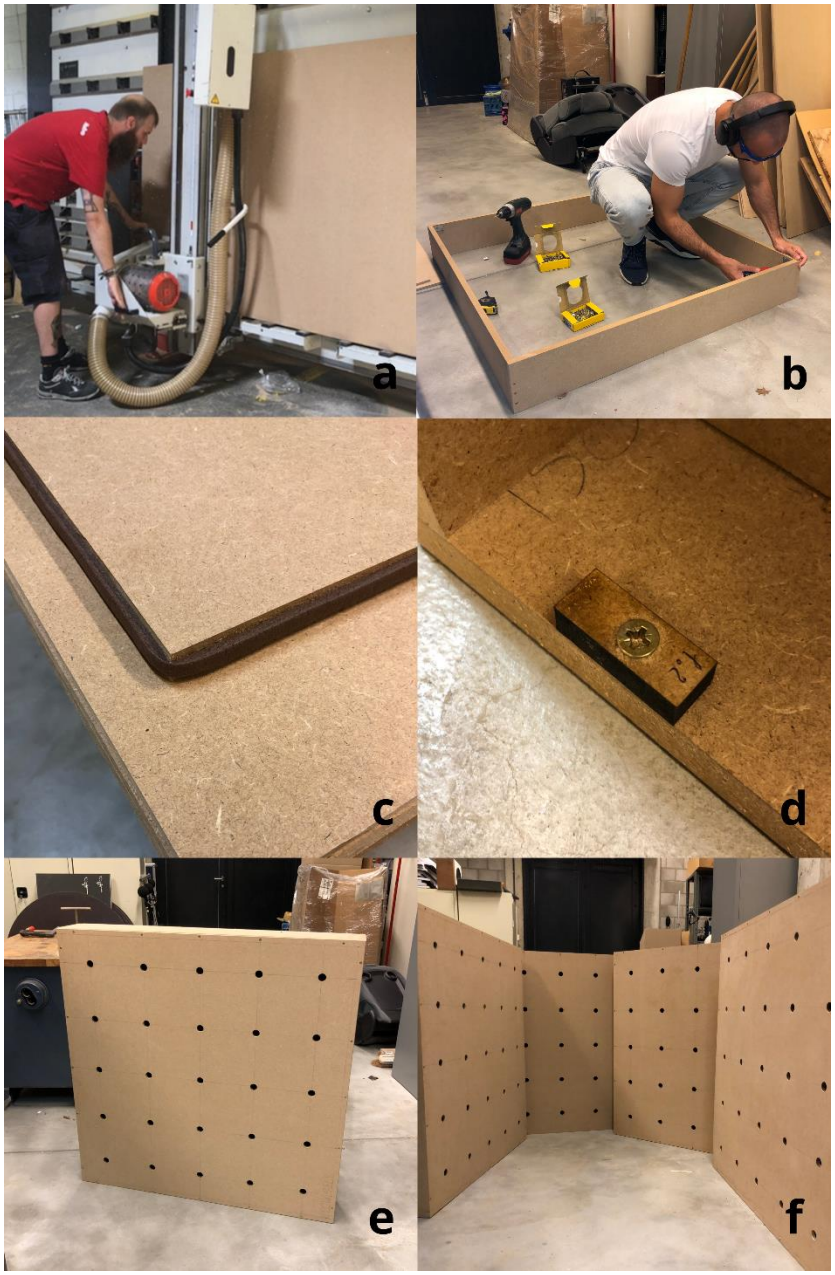


**Figure 42**: Construction of the resonator

## *3.5 Anechoic room*

This section reports the impulse responses measured in an anechoic chamber. The reference measurement is followed by the responses of the resonator as the cavity depth *d* varies and the measurement of the rigid reflection performed at the maximum depth of 120 mm. **Figure 43** shows the sound pressure levels measured for various depths of the resonator cavity.

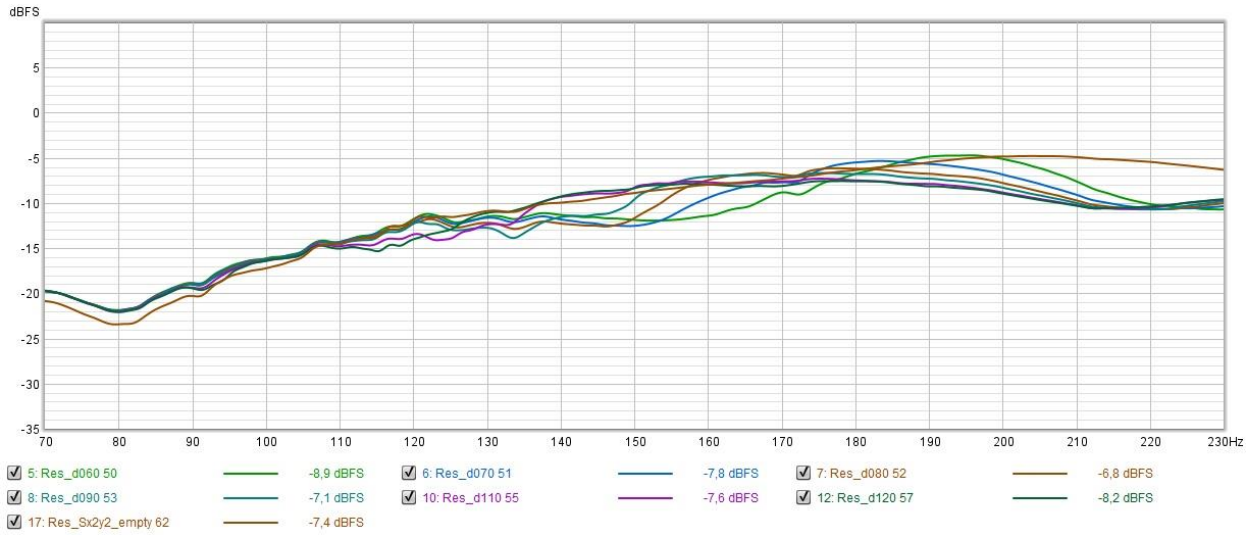


**Figure 43**: Measurements in the anechoic chamber of SPLs for various depths of the resonator

In the frequency range of our interest, the RIRs influenced by two very different cavity depths and by the rigid reflection of the panel are compared, as shown in **Figure 44**.

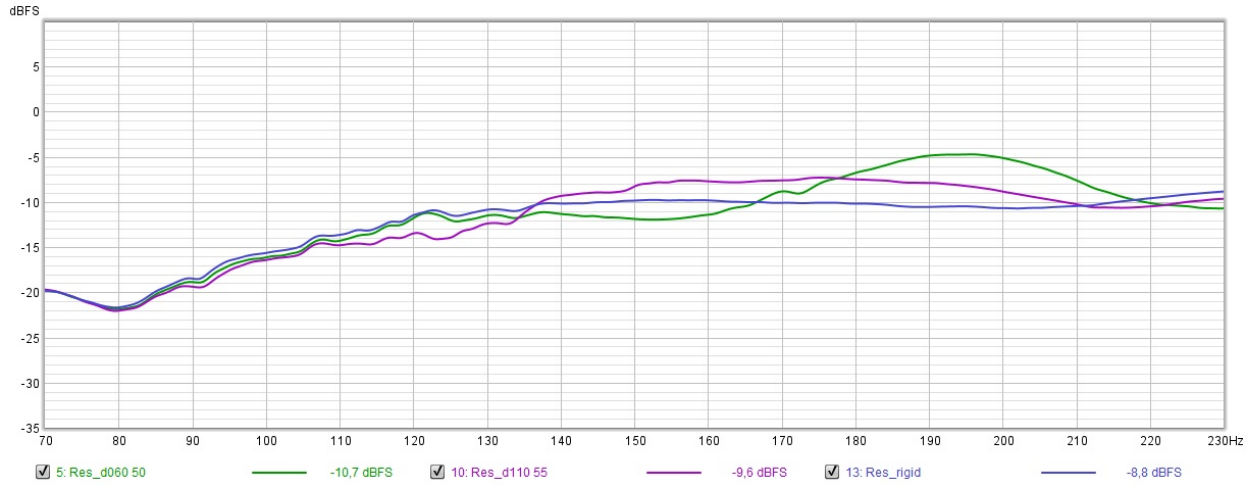


**Figure 44**: Comparison of SPLs for two different cavity depths and with a hard cover

## *3.7 Reverberation Room*

In the reverberation chamber, a total of 24 RIRs are measured., utilizing the 6 measurement positions. 12 measurements are carried out with the empty room, 6 for each source position, and an equal number with the sample inside the room. By acquiring data on reverberation times, information about the absorption of the Device Under Test (DUT) is obtained.  shows the absorption coefficient calculated for the average reverberation times of the reference (empty room) and those influenced by the undamped Helmholtz resonator.

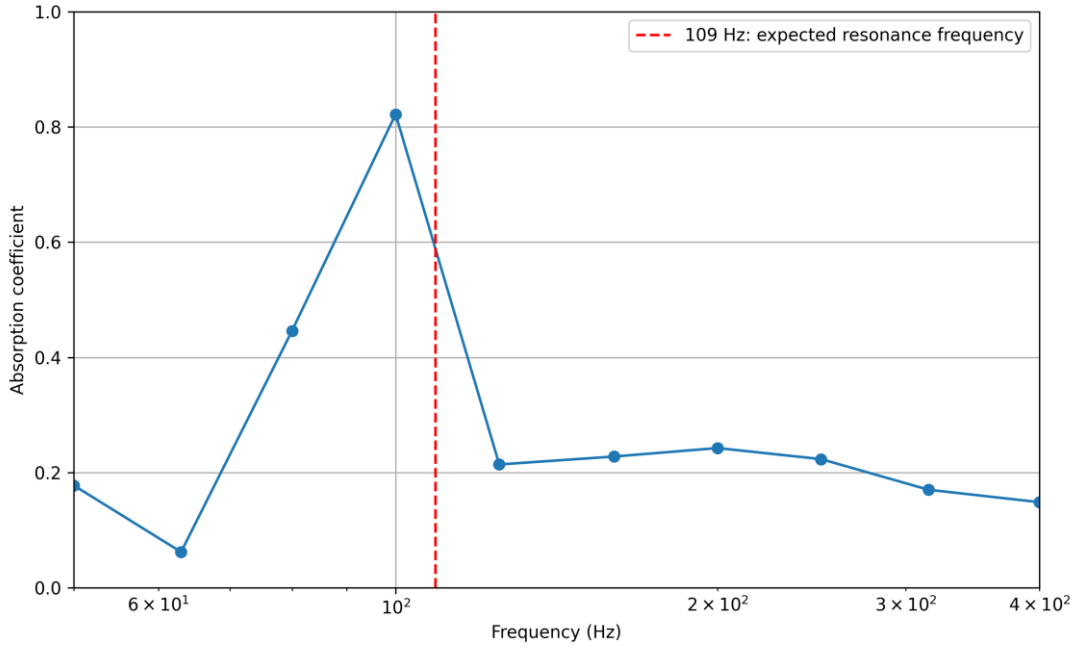


**Figure 45**: Absorption coefficient of the Helmholtz resonator

# 4 Discussion of the results

## *4.1 Preliminary simulations and measurements*

The simulation carried out with AMROC for a rectangular geometric environment and the simulation performed in Ansys produced very close results, confirming, at least theoretically, the validity of the approximated regular model. It is estimated that the vertical theoretical modes correspond to frequencies of 41, 82, and 125 Hz. In order to tune the resonator to a frequency not too low to avoid difficulties in managing frequencies, nor too close to the diffuse behavior of the sound field, the theoretical mode 0-0-3, approximately at 125 Hz, is chosen as a possible candidate for tuning the resonator.

Given the pressure distribution characteristics of the selected mode, the measurement taken in the semi-reverberant chamber in position 1 is particularly significant, as the sound pressure is recorded at points where one would expect to find the nodes and antinodes of the resonant frequency on the z-axis.

However, from the measurement taken at ground level, it would seem that a fairly strong mode manifests around 111 Hz. As the nodes should be located at half the wavelengths, by calculating that the wavelength is $\lambda = c/f = 340/111 \approx 3$, it is possible to state that the vertical mode occurs at this frequency. To investigate, the three measurements taken at the same point but with the microphone positioned at three different heights are compared. It is observed that the mode is distinctly perceptible with the microphone placed near the floor, attenuates slightly when measured at 110 cm, and becomes almost imperceptible at a height of 200 cm.

This variation in the perception of the mode at different heights confirms that sound energy is concentrated in specific horizontal layers within the room. Since it is expected that the plane of nodes is located at approximately 137 cm in height and that the position at 200 cm corresponds to a point near the central belly of the vertical mode, this pattern, depicted in **Figure 46**, aligns with the expectations of the theoretical vertical mode 0-0-3.

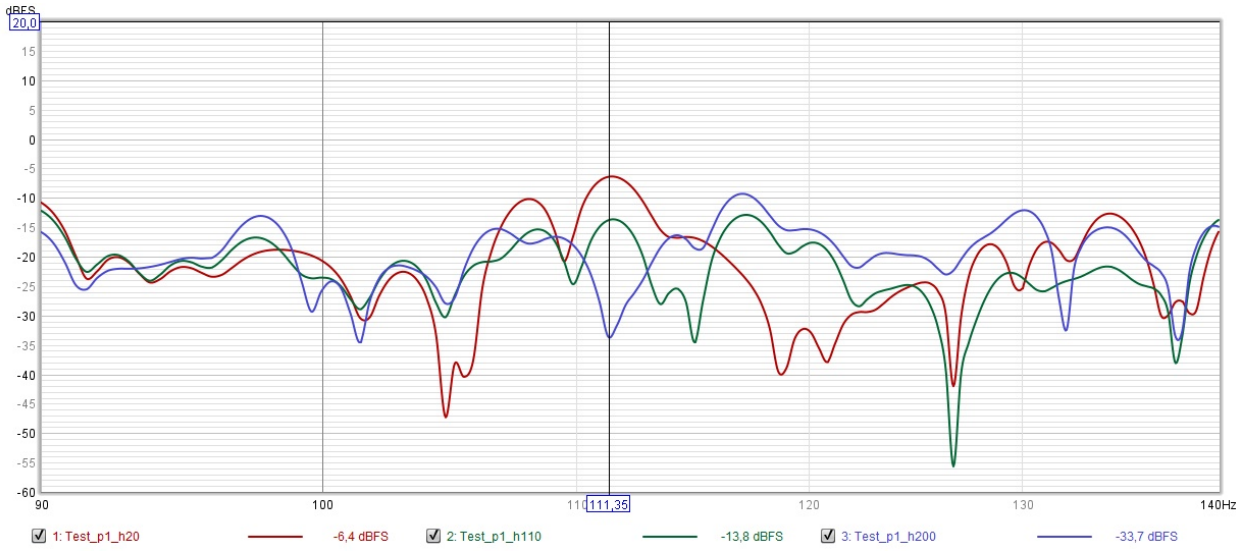


**Figure 46**: SPL of the three central measurements between 90 and 140 Hz

Another check can be performed by comparing all measurements taken in the environment in different configurations at the specific frequency of 111 Hz. Since the energy is distributed in a horizontal layer near the floor, we expect to find high sound pressure levels in all measurements, although they may be slightly lower than the measurement from the first configuration, where the maximum energy concentration is expected. Instead, we expect the sound pressure levels to be higher than the measurement taken in the center of the room at a height of 110 cm, as this

position is farther from the node and therefore less influenced by the maximum energy concentration.

From the analysis of the graph in **Figure 47**, which shows the SPL curves of all nine measurements, it can be observed that in all measurements taken at points other than the center of the room, the sound pressures at 111 Hz are lower than the pressure recorded at floor level in position 1 and higher than that measured at a height of 110 cm in the same position. This behavior suggests that the frequency of 111 Hz consistently manifests itself, confirming what would be the behavior of the theoretical distribution of the sound energy of the vertical mode.

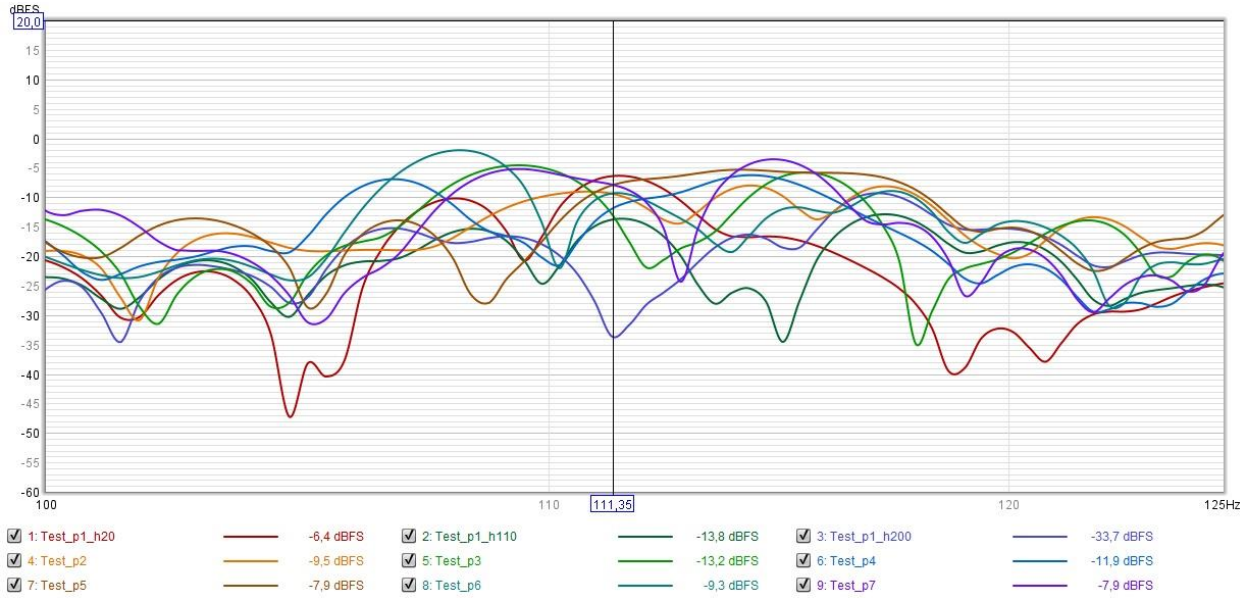


**Figure 47**: RIRs of the semi-reverberant room for all measurements

Despite registering a significant pressure around 125 Hz in measurement 1, the acoustic response associated with that frequency in the rest of the positions differs from what a vertical mode would exhibit. Therefore, the most likely hypothesis is that 111 Hz corresponds to the theoretical mode 0-0-3. However, considering that the piston mechanism envisaged for the resonator allows for the adjustment of the resonance frequency of the device, the theoretical mode at 125 Hz is chosen as the target frequency for tuning the HR, even though it is less evident from the results of the experimental measurements.

## *4.2 Resonator design*

For the construction of the HR, medium-density fiberboard (MDF) has been chosen as the material, preferred for its uniformity and ease of processing compared to traditional wood. The perforated panel has a thickness $t$ = 9 mm, determined based on the availability of commercial materials. The spacing between the holes $D$ is initially set to 100 mm, equal to the impedance tube section where the samples will be tested. Since the maximum size of the resonator is set at 150 mm for logistical and practical reasons, the maximum cavity depth $d$ of the resonator is then fixed at 120 mm. This is because 18 mm corresponds to the thickness of the piston plate, while the blocks to prevent its exit and to adjust its depth correspond to 12 mm. To fully utilize this mechanism, it is decided to find a value of aa such that the cavity depth is approximately half of its maximum extension, estimating that it never exceeds 50 mm at its maximum compression. Relying on this mechanism, which allows for quick tuning adjustment of the resonator, the theoretical frequency of 125 Hz is chosen as the target frequency for the device. Through simulation, it is estimated that for a cavity depth between 80 and 90 mm, the radius of the resonator holes should be between 4 and 5 mm. However, already from the first measurement in the impedance tube, it becomes apparent that this sample does not meet the requirements at all, as

its resistance is greater than 415 Rayls and its behavior is inconstant. The surface impedance, which ideally should range between 0 and 415 Rayls across the entire frequency spectrum of interest, exhibits non-optimal behavior. The measurements of samples with hole diameters equivalent to 5, 6, and 7 mm reveal that behavior meeting the design requirements is achieved only starting from a = 7 mm. Therefore, new samples with a larger diameter are created, and from their testing, it emerges that the surface impedance Z exhibits optimal behavior. However, the anticipated increase in diameter leads to a recalibration of the Helmholtz resonator parameters. Since with a hole spacing $D$ = 100 mm and a minimum $a$ of 7, the resonance frequency of the device reaches and exceeds the low-frequency limit, it is necessary to increase $D$ to a value that allows tuning of the resonator within the target frequency range. The hole spacing is therefore set to 200 mm to maintain consistency with the previous value and with the size of the impedance tube, and to simplify the design of the perforated panel. Indeed, with a spacing of 200 mm, the number of holes, although reduced from 49 to 25, maintains its homogeneous distribution, even when combining multiple resonators. In the compact configuration, the four resonators form a 2x2 resonator that maintains a hole spacing $D$ = 200 mm. Theoretical HRs corresponding to the measured holes in the impedance tube are then calculated, and samples are tuned to the target frequency. Then, the expected values of absorption coefficient $\alpha$, porosity $\varepsilon$, resistance $r_m$, and the product $\varepsilon \cdot r_m$ are compared with those obtained experimentally. The graph shows, as expected, that the values of resistance and their products for the respective porosities decrease as $a$ increases.

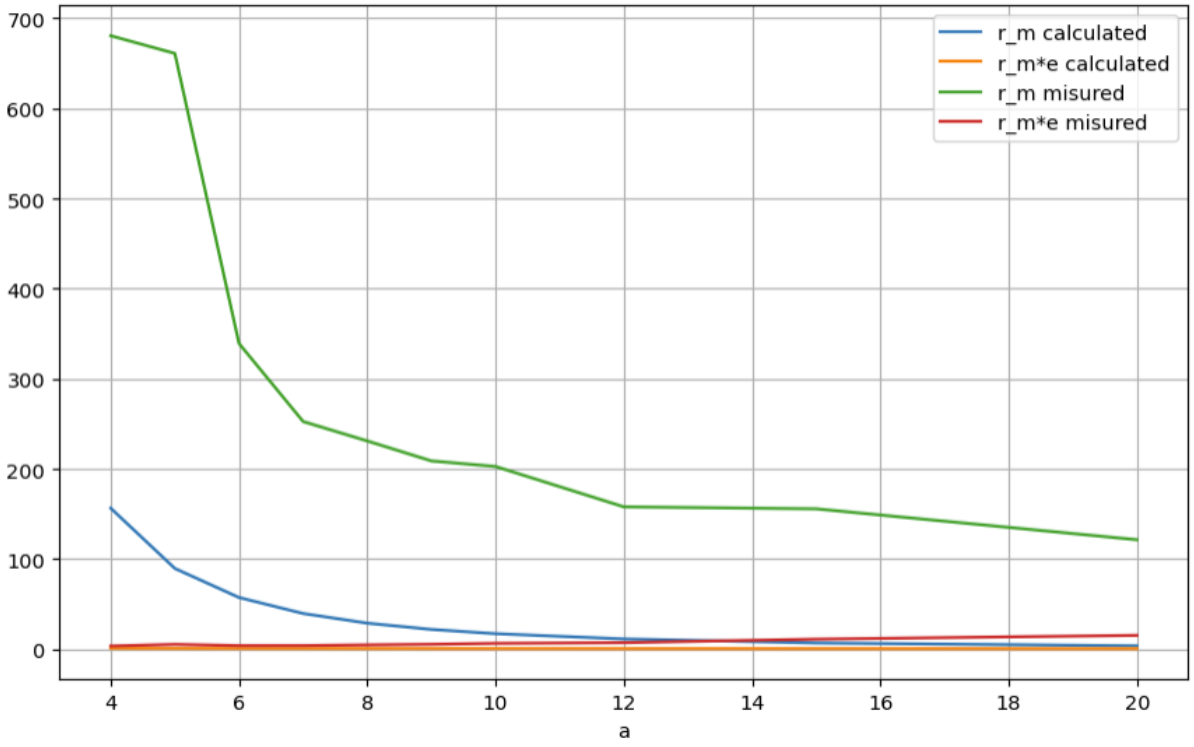


**Figure 48**: Behavior of the calculated and experimentally measured resistance, and of their product by the porosity, as a function of the size of $a$

Given the equal validity of their acoustic impedance, the sample with a hole radius of 12.5 mm has been chosen as the final specimen. This decision is motivated by the optimal cavity depth of 88 mm for absorbing the target frequency. This value gives the piston plenty of room to move, both in compression and extension directions. Another factor considered, far from negligible, is the size of the available drills. With a drill bit diameter of approximately 25.4 mm at our disposal,

choosing this hole size should minimize instrumentation error, thus improving the reliability of the results.

### *4.3 Anechoic Room*

The measurements conducted in an anechoic chamber showed a slight decrease in sound pressure levels centered around a frequency slightly higher than the target frequency when transitioning from a depth d of 60 mm to 120 mm. However, these pressure drops provide no information and do not directly show the absorption characteristics of the device.

Therefore, it is not possible to conclude relevant information from these measurements, at least regarding the resonant frequency of the resonator. More in-depth measurements on the effects of rigid reflection could be useful to evaluate the phenomenon of destructive interference.

### *4.4 Test in the semi-reverberant room*

The HR has been designed to absorb a wide range of frequencies thanks to the piston mechanism allowing dynamically changing the resonance frequency of the absorber, spanning approximately between 108 Hz for $d$ = 120 mm to 170 Hz for $d$ = 50 mm. Having to specifically absorb the 111Hz of the semi-reverberant room, and since from some initial, albeit inconclusive, measurements in an anechoic room it seemed that the absorption occurs at a slightly higher frequency than expected, it is advisable to set d directly to the depth maximum (120 mm) to bring the absorption peak as close as possible to the 111 Hz frequency.

Measurements with three configurations of the four HRs are then carried out. The first tested configuration involves the four resonators being arranged at the center, effectively creating a single large resonator. This configuration is intended to examine how cohesively the resonators can function when closely grouped together and their collective influence on the acoustic environment. The second configuration adopts a checkerboard pattern. This arrangement aims to disperse the resonators more evenly throughout the room, potentially offering a different interaction with the room's acoustic modes. By dispersing the resonators, the hypothesis is to achieve a more uniform distribution of acoustic absorption throughout the room. The third and final configuration places one resonator in each corner of the room, where it is presumed that the energy accumulation is maximum. The variety of data collected through these measurements should allow us to estimate the effectiveness of the resonator with a good approximation.

From the measurements made in configuration 1, it is evident that the absorption of the undamped Helmholtz resonator with maximum cavity depth occurs at 111-112 Hz, providing maximum damping of 20 dB and almost completely absorbing the vertical mode.

The pressure ratio graphs provide crucial information on the effectiveness of the resonators. It is observed that, despite some differences, the resonators effectively fulfill their predetermined function. Through measurements conducted with the resonators arranged in the compact version (configuration 1), with the source positioned at s1, the effectiveness of the resonators in causing a significant decrease in acoustic pressure is highlighted, reaching values of -14/-18 dB. Interestingly, maximum absorption occurs when the microphone is positioned at the center of the configuration, rather than at the center of a single resonator. Additionally, there is notable effectiveness of the checkerboard configuration 2 compared to configuration 3, which involves placing the resonators in the corners of the room.

The latter configuration does not show a significantly different impact with 3 or 4 resonators. A different result is obtained when, in configuration 1, the source is positioned at s2, which is above the resonator. In this case, the proximity between the microphone, source, and sample leads to absorption, although this is characterized by a narrower bandwidth and a higher frequency shift. Overall, the resonators effectively perform their function. In particular, analyzing the average transfer function of all measurements taken at ground level reveals a well-defined absorption. This result confirms the initial hypothesis regarding the emergence of side peaks around the absorption frequency and the possibility to redistributing modes across parts of the floor.

### *4.5 Reverberation chamber*

The absorption coefficient graph calculated following the measurements taken in the anechoic chamber, as shown in the Figure, reveals the last fundamental data about the tested HRs: the resonance frequency. The graph highlights a pronounced peak at around 100 Hz. Since the expected resonance frequency is approximately 109 Hz, and the graph is in third-octave bands, this absorption would visually collapse around 100 Hz. Therefore, this measurement not only demonstrates the effectiveness of the device in absorbing low frequencies but also the alignment of the actual resonance frequency with the theoretically expected one.

# 5 Conclusions

In the context of this thesis, a weakly damped Helmholtz resonator was designed and built to demonstrate the potential of modal redistribution of these devices. The choice of frequency to tune the device to was made following the analysis of the test room. To do this, the room was first analyzed using simple analytical models (AMROC) and numerical models (Ansys), and finally measured. The analyses showed a significant correspondence between the theoretical modes generated by ANSYS simulations on a complex three-dimensional model and those derived through AMROC for a rectangular room, the dimensions of which were calculated using Bretschneider's Theorem. Following theoretical analyses and empirical measurements, the targeted frequency was a vertical axial mode, as it could be more easily and effectively measured.

The weakly damped resonator was designed using a 1D analytical model and impedance tube measurements. Following tests on numerous samples, during which the instrument confirmed its effectiveness in accurately determining surface impedance values, and through accurate simulations, full-scale resonators were built. The introduction of a piston mechanism in the resonator emphasized the importance of flexibility and dynamic tuning of the resonance frequency to adapt to environmental variations and design discrepancies. In this experiment, the ability to adjust the depth of the cavity played a crucial role, enabling successful conduct of the investigation in a semi-reverberant environment and examination of the device's influence on the space's acoustics.

The four resonators provided a valid scientific sample, and the project was further verified through measurements in a reverberation chamber. The effect on room modes was revealed and studied for different configurations of the resonators, and the phenomenon of modal splitting was observed as in simulations, confirming the possibility of redistributing modes across parts of the floor. Following analysis conducted in the reverberation chamber, a correspondence between the predicted and actual resonance frequency was confirmed.

The thesis demonstrates the potential of applying HR for low-frequency modal redistribution, and further research should focus on additional experimental, numerical, and perceptual verification of this application.

## References


[1] M. A. Biot, «Theory of propagation of elastic waves in a fluid-saturated porous solid. II. Higher frequency range,» *J. Acoust. Soc. Am.,* vol. 28, p. 179–191, 1956.

[2] T. Dupont, P. Leclaire, O. Sicot, X. L. Gong e R. Panneton, «Acoustic properties of air-saturated porous materials containing dead-end porosity,» *J Appl Phys,* vol. 110, n. 094903, 2011.

[3] L. Cao, Q. Fu, Y. Si, B. Ding e J. Yu, «Porous materials for sound absorption,» *Compos Commun,* vol. 10, pp. 25-35, 2018.

[4] H. Zhao, Y. Wang, D. Yu, H. Yang, J. Zhong, F. Wu e J. Wen, «A double porosity material for low frequency sound absorption,» *Compos Struct,* vol. 239, n. 111978, 2020.

[5] G. Ji, Y. Fang e J. Zhou, «Porous acoustic metamaterials in an inverted wedge shape,» *Extreme Mech Lett,* vol. 36, n. 100648, 2020.

[6] U. Ingard, «On the theory and design of acoustic resonators,» *J Acoust Soc Am,* vol. 25, pp. 1037-61, 1953.

[7] S. R. Kim, Y. H. Kim e J. H. Jang, «A theoretical model to predict the low-frequency sound absorption of a Helmholtz resonator array,» *J Acoust Soc Am,* vol. 119, p. 1933–6, 2006.

[8] N. Gao, S. Qu, J. Li e W. Chen, «Harnessing post-buckling deformation to tune sound absorption in soft Helmholtz absorbers,» *Int J Mech Sci,* vol. 208, n. 106695, 2021.

[9] A. Komkin, M. Mironov e A. Bykov, «Sound absorption by a Helmholtz resonator,» *Acoust Phys,* vol. 63, p. 385–392.

[10] H. Hoppen, F. Langfeldt, W. Gleine e O. Von Estorff, «Helmholtz resonator with two resonance frequencies by coupling with a mechanical resonator,» *J Sound Vib,* vol. 559, n. 117747, 2023.

[11] D. Y. Maa, «Potential of microperforated panel absorber,» *J Acoust Soc Am,* vol. 104, p. 2861–6, 1998.

[12] D. H. Lee e Y. P. Kwon, «Estimation of the absorption performance of multiple layer perforated panel systems by transfer matrix method,» *J Sound Vib,* vol. 278, pp. 847-60, 2004.

[13] Y. Y. Lee, E. W. M. Lee e C. F. Ng, «Sound absorption of a finite flexible micro-perforated panel backed by an air cavity,» *Sound Vib,* vol. 278, pp. 847-60, 2005.

[14] Y. Y. Lee e E. W. M. Lee, «Widening the sound absorption bandwidths of flexible micro-perforated curved absorbers using structural and acoustic resonances,» *Int J Mech Sci,* vol. 49, pp. 925-34, 2007.

[15] Y. Y. Lee, «The effect of leakage on the sound absorption of a nonlinear perforated panel backed by a cavity,» *Int J Mech Sci,* vol. 107, pp. 242-52, 2016.

[16] H. S. Kim, P. S. Ma, S. R. Kim, S. H. Lee e Y. H. Seo, «A model for the sound absorption coefficient of multi-layered elastic micro-perforated plates,» *J Sound Vib,* vol. 430, pp. 75-92, 2018.

[17] X. Liu, C. Wang, Y. Zhang e L. Huang, «Investigation of broadband sound absorption of smart micro-perforated panel (MPP) absorber,» *Int J Mech Sci,* vol. 199, n. 106426, 2021.

[18] C. Wang e L. Huang, «On the acoustic properties of parallel arrangement of multiple micro-perforated panel absorbers with different cavity depths,» *J Acoust Soc Am,* vol. 130, pp. 208-18, 2011.

[19] H. S. Kim, P. S. Ma, B. K. Kim, S. R. Kim e S. H. Lee, «Low-frequency sound absorption of elastic micro-perforated plates in a parallel arrangement,» *J Sound Vib,* vol. 460, n. 114884, 2019.

[20] U. Ackermann, H. Fuchs e N. Rambausek, «Sound absorbers of a novel membrane construction,» *Appl Acoust,* vol. 25, pp. 197-215, 1988.

[21] D. Jun, J. Plasek, M. Rychtarikova e C. Glorieux, «Room modes in rectangular rooms with complex impedance boundaries,» in *Juniorstav 2024*, Brno, Czech republic, 2024.

[22] T. J. Cox e P. D'Antonio, Acoustic Absorbers and Diffusers. Theory, design and application, New York: Taylor & Francis, 2009.

[23] W. C. Sabine, Collected Papers on Acoustics, Harvard University Press (1922); Acoustical Society of America (1993).

[24] C. F. Eyring, «Reverberation time in 'dead' rooms,» *J. Acoust. Soc. Am.,* vol. 1, pp. 217-26, 1930.

[25] G. Millington, «A modified formula for reverberation,» *J. Acoust. Soc. Am.,* vol. 4, pp. 69-81, 1932.

[26] S. Stansfeld e M. Matheson, «Noise pollution: non-auditory effects on health,» *BrMed Bull,* vol. 68, pp. 243-257, 2003.

[27] A. Seddigh, E. Berntson, F. Jönsson, H. Westerlund e C. Bodin Danielson, «The effect of noise absorption variation in open-plan offices: A field study with a cross-over design,» *J Environ Psychol,* vol. 44, pp. 34-44, 2015.

[28] W. Passchier-Vermeer e W. F. Passchier, «Noise Exposure and Public Health,» *The National Institute of Environmental Health Sciences,* pp. 123-131, 2000.

[29] S. Abbaszadech, L. Zagreus, D. Lehrer e C. Huizenga, «Occupant satisfaction with indoor environmental quality in green buildings,» in *Proceedings, Healthy Buildings 2006*, Lisbon, Portugal, 2006.

[30] B. Berglund, P. Hassmen e R. S. Job, «Sources and effects of low-frequency noise,» *J Acoust Soc Am,* vol. 99(5), pp. 2985-3002, 1996.

[31] K. P. Waye, «Effects of low frequency noise and vibrations: environmental and occupational perspectives,» in *In: Nriagu JO (ed) Encyclopedia of environmental health*, Burlington, Elsevier, 2011, pp. 244-253.

[32] H. G. Leventhall, «Low frequency noise and annoyance,» *Noise Health,* vol. 6(23), pp. 59-72, 2004.

[33] W. Babisch, H. Ising e G. J, «Health status as a poten tial effect modifier of the relation between noise annoyance and incidence of ischaemic heart disease,» *Occup Environ Med,* vol. 60(10), pp. 739-745, 2003.

[34] C.-H. Chiu, S.-C. Lung, N. Chen, J.-S. Hwang e M.-C. Tsou, «Effects of low-frequency noise from wind turbines on heart rate variability in healthy individuals,» *Sci Rep,* vol. 11, n. 17817, 2021.

[35] S. Kumar e H. P. Lee, «The Present and Future Role of Acoustic Metamaterials for Architectural and Urban Noise Mitigations,» *Acoustics,* vol. 1(3), pp. 590-607, 2019.

[36] L. Chang, A. Jiang, M. Rao, F. Ma, H. Huang, Z. Zhu, Y. Zhang, Y. Wu, B. Li e Y. Hu, «Progress of low-frequency sound absorp tion research utilizing intelligent materials and acoustic metama terials,» *RSC Adv,* vol. 11(69), p. 37784–37800, 2021.

[37] H. Kuttruff, Room Acoustics, Spon Press, 2000.

[38] P. M. Morse e H. Feshbach, Methods of Theoretical Physics, McGraw-Hill, New York: McGraw-Hill, 1953.

[39] P. M. Morse e K. U. Ingard, Theoretical Acoustics, New York: McGraw-Hill, 1968,.

[40] M. R. Schroeder e H. Kuttruff, «On frequency response curves in rooms. Comparison of experimental, theoretical, and Monte Carlo results for the average frequency spacing between maxima,» *J. Acoust. Soc. Am.,* vol. 34(1), pp. 76-80, 1962.

[41] M. R. Schroeder, Acustica, 1954.

[42] F. J. Fahy, Foundations of engineering acoustics, London: Elsevier, 2000.

[43] A. Selamet e I. Lee, «Helmholtz resonator with extended neck,» *J Acoust Soc Am,* vol. 113(4), p. 1975–1985, 2003.

[44] S. Huang, X. Fang, X. Wang, B. Assouar, Q. Cheng e Y. Li, «Acoustic perfect absorbers via Helmholtz resonators with embedded apertures,» *J Acoust Soc Am ,* vol. 145(1), p. 254–262, 2019.

[45] J. Guo, X. Zhang, Y. Fang e Z. Jiang, «A compact low-fre quency sound-absorbing metasurface constructed by resonator with embedded spiral neck,» *Appl Phys Lett,* vol. 117(22), n. 221902, 2020.

[46] C. Song, S. Huang, Z. Zhou, J. Zhang, B. Jia, C. Zhou, Y. Li e Y. Pan, «Perfect acoustic absorption of Helmholtz resonators via tapered necks,» *Appl Phys Express,* vol. 15(8), n. 084006.

[47] M. Alster, «Improved calculation of resonant frequencies of Helmholtz resonators,» *J Sound Vib,* vol. 24(1), p. 63–85, 1972.

[48] R. Chanaud, «Effects of geometry on the resonance frequency of Helmholtz resonators,» *J Sound Vib,* vol. 178(3), p. 337–348, 1994.

[49] A. Selamet, P. M. Radavich, N. Dickey e J. Novak, «Circular concentric Helmholtz resonators,» *J Acoust Soc Am,* vol. 101(1), p. 41–51, 1997.

[50] A. Selamet e Z. L. Ji, «Circular asymmetric Helmholtz resonators,» *J Acoust Soc Am,* vol. 107(5), p. 2360–2369, 2000.

[51] R. Randeberg, «A Helmholtz resonator with a lateral elon gated orifice,» *Acta Acust Acust,* vol. 86(1), p. 77–82, 2000.

[52] S. Huang, Z. Zhou, D. Li, T. Liu, X. Wang, J. Zhu e Li, «Compact broadband acoustic sink with coherently coupled weak resonances,» *Science Bulletin,* vol. 65(5), pp. 373-379, 2020.

[53] V. Rajendran, A. Piacsek e T. Méndez Echenagucia, «Design of broadband Helmholtz resonator arrays using the radiation impedance method,» *The Journal of the Acoustical Society of America,* vol. 151, pp. 457-466, 2022.

[54] S. H. Baek, J. Y. Jang, K. J. Song e S. H. Park, «Design of flat broadband sound insulation metamaterials by combining helmholtz resonator and fractal structure,» *Journal of Mechanical Science and Technology,* vol. 35(7), pp. 2809-2817, 2021.

[55] S. Huang, X. Fang, X. Wang, B. Assouar, Q. Cheng e Y. Li, «Acoustic perfect absorbers via spiral metasurfaces with embedded apertures,» *Applied Physics Letters,* vol. 113(23), n. 233501, 2018.

[56] J. Guo, X. Zhang, Y. Fang e Z. Jiang, «Wideband low-fre quency sound absorption by inhomogeneous multi-layer resona tors with extended necks,» *Compos Struct,* vol. 260, n. 113538, 2021.

[57] K. Mahesh e R. S. Mini, «Theoretical investigation on the acoustic performance of Helmholtz resonator integrated micro perforated panel absorber,» *Appl Acoust,* vol. 178, n. 108012, 2021.

[58] C. Boutin e F. X. Becot, «Theory and experiments on poro acoustics with inner resonators,» *Wave Motion ,* vol. 54, p. 76–99, 2015.

[59] J. Dandsena e D. Jena, «Acoustic attenuation and effective properties of single and periodic Helmholtz resonators having porous core,» *Appl Acoust,* vol. 211, n. 109490, 2023.

[60] N. Jiménez, V. Romero-García, V. Pagneux e J. P. Groby, «Rainbow-trapping absorbers: broadband, perfect and asymmet ric sound absorption by subwavelength panels for transmission problems,» *Sci Rep,* vol. 7(1), p. 1–12, 2017.

[61] J. Mei, G. Ma, M. Yang, Z. Yang, W. Wen e P. Sheng, «Dark acoustic metamaterials as super absorbers for low-frequency sound,» *Nat Commun ,* vol. 3, n. 756, 2012.

[62] G. Ma, M. Yang, S. Y. Z. Xiao e P. Sheng, «Acoustic metasurface with hybrid resonances,» *Nat Mater,* vol. 13, p. 873–878, 2014.

[63] J. Li, W. Wang, Y. Xie, B. Popa e S. Cummer, «A sound absorbing metasurface with coupled resonators,» *Appl Phys Lett,* vol. 109, n. 091908, 2016.

[64] H. Ryoo e W. Jeon, «Dual-frequency sound-absorbing metasurface based on visco- thermal effects with frequency dependence,» *J Appl Phys,* vol. 123, n. 115110., 2018;.

[65] H. Ryoo e W. Jeon, «Perfect sound absorption of ultra-thin metasurface based on hybrid resonance and space-coiling,» *Appl Phys Lett,* vol. 113, n. 121903, 2018.

[66] J. Kim e W. Jeon, «Nonplanar metasurface for perfect absorption of sound waves,» *J Acoust Soc Am ,* vol. 149, p. 2323–36, 2021.

[67] X. Cai, Q. Guo, G. Hu e J. Yang, «Ultrathin low-frequency sound absorbing panels based on coplanar spiral tubes or coplanar Helmholtz resonators,» *Appl Phys Lett,* vol. 105, n. 121901, 2014.

[68] Y. Li e B. M. Assouar, «Acoustic metasurface-based perfect absorber with deep subwavelength thickness,» *Appl Phys Lett,* vol. 108, n. 063502, 2016.

[69] C. Chen, Z. Du, G. Hu e J. Yang, «A low-frequency sound absorbing material with subwavelength thickness,» *Appl Phys Lett ,* vol. 110, n. 221903, 2017.

[70] Y. Shen, Y. Yang, X. Guo, Y. Shen e D. Zhang, «Low-frequency anechoic metasurface based on coiled channel of gradient cross-section,» *Appl Phys Lett,* vol. 114, n. 083501, 2019.

[71] T. Yasuda, C. Wu, N. Nakagawa e K. Nagamura, «Studies on an automobile muffler with the acoustic characteristic of low-pass filter and Helmholtz resonator,» *Appl Acoust,* vol. 74(1), p. 49–57, 2013.

[72] T. Li, «Literature review of tire-pavement interaction noise and reduction approaches,» *J Vibroeng,* vol. 20(6), p. 2424–2452, 2018.

[73] S. Park, «Acoustic properties of micro-perforated panel absorbers backed by Helmholtz resonators for the improvement of low-frequency sound absorption,» *J Sound Vib ,* vol. 332(20), p. 4895–4911, 2013.

[74] M. Dannemann, M. Kucher, E. Kunze, N. Modler, K. Knobloch, L. Enghardt, E. Sarradj e K. Höschler, «Experimental study of advanced Helmholtz resonator liners with increased acoustic performance by utilising material damping effects,» *Appl Sci,* vol. 8(10), n. 1923, 2018.

[75] D. May, K. Plotkin, R. Selden e B. Sharp, «Lightweight side walls for aircraft interior noise control,» National Aeronautics and Space Administration (NASA), 1985.

[76] V. Rajendran, T. Méndez Echenagucia e A. Piacsek, «Design of sound absorptive metamaterials with shared waveguides by means of numerical analysis and analytical modeling,» in *Forum Acusticum 2023*, Torino, 2023.

[77] International Organization for Standardization, *ISO 10534-2:1998, Acoustics – Determination of sound absorption coefficient and impedance in impedance tubes. Part 1: Method using standing wave ratio,* 1998.

[78] International Organization for Standardization, *ISO 10534-2:1998, Acoustics – Determination of sound absorption coefficient and impedance in impedance tubes. Part 2: Transfer-function method,* 1998.

[79] L. Cremer e H. A. Müller, Principles and Applications of Room Acoustics, Applied Science

Publishers, 1978.

[80] A. W. Guess, «Result of impedance tube measurements on the acoustic resistance and reactance,» *J. Sound Vib,* n. 40, p. 119–37, 1975.

[81] L. E. Kinsler, A. R. Frey, A. B. Coppens e J. V. Sanders, Fundamentals of Acoustics, 4th edn, John Wiley & Sons, 2000.

[82] S. Muller e M. P, «Transfer Function Measurement with Sweeps,» *Journal of the Audio Engineering Society,* vol. 49, pp. 443-471, 2001.

[83] A. Farina, «Simultaneous Measurement of Impulse Response and Distortion with a Swept-sine technique,» in *108th AES Convention*, Paris, 2000.

[84] D. Griesinger, «Beyond MLS – Occupied Hall Measurement with FFT Techniques,» in *101st AES convention*, Los Angeles, 1996.

[85] D. Jun, «Imptube,» https://github.com/vyhyb/imptube, Brno.

## List of Figures

## List of Tables